Hindawi
Geofluids
Volume 2019, Article ID 3781410, 26 pages
https://doi.org/10.1155/2019/3781410

Research Article

Evaporation-Induced Water and Solute Coupled Transport in Saline Loess Columns in Closed and Open Systems

Jian Xu,[1,2] **Wei Lan**,[1] **Yanfeng Li**,[1] **Wen-Chieh Cheng**,[1,2] **Jun Yuan**,[3] **and Qinghai Tan**[4]

[1]*School of Civil Engineering, Xi'an University of Architecture and Technology, Xi'an, Shaanxi 710055, China*
[2]*Shaanxi Key Laboratory of Geotechnical and Underground Space Engineering, Xi'an University of Architecture and Technology, Xi'an, Shaanxi 710055, China*
[3]*Northwest Electric Power Design Institute Co., Ltd. of China Power Engineering Consulting Group, Xi'an, Shaanxi 710075, China*
[4]*Qinghai Electric Power Design Institute of Co. Ltd. of China Electric Power Construction Group, Xining, Qinghai 810008, China*

Correspondence should be addressed to Jian Xu; xujian@xauat.edu.cn

Received 1 June 2019; Accepted 30 August 2019; Published 10 December 2019

Academic Editor: Micòl Mastrocicco

Evaporation-induced water and solute coupled transport is a significant cause for soil salinization that leads to a series of engineering and environmental problems. In the artificial evaporation environment, including relative humidity, atmospheric temperature, atmospheric pressure, radiation intensity, and wind speed, evaporation of loess columns with sodium sulfate, temperature profile, and water and solute transport in closed and open systems were investigated. In the former case, a range of stability was noted in the lower part of the column where the heat, water, and solute coupled transport only exhibited a weak response to a specified evaporation environment. As the environment was more favorable for evaporation, or at a higher gradient of temperature, this range extended downwards, while above this range the heat, water, and salt profiles in the evaporation-affected domain changed dramatically, characterized by a basic law that solutes moved with water and were then retained with water desalinated. Evidences were found from the profiles that the water contents in the evaporation-affected range decreased but the salt contents increased, especially in the surface. In an open system, by contrast, there was little difference in temperature but greater in water and salt profiles. Three stages were found from the supply of external water during evaporation. In the initial stage, the higher gradient formed between the initial moisture state and the preset external water level led to a rapid supply of external water. As the evaporation proceeded, a relatively stable water profile was reached as the intensity of water supply approached to that of evaporation, accompanied by a continual migration of solutes towards the surface. Due to the accumulation of precipitated salts, water transport was slowed down, and the intensity of water supply decreased. The changes in soil suction may account for the above behavior.

1. Introduction

The Loess Plateau in China is often covered with deep loess, with dry surface soils due to the not well-developed surface water system and deep groundwater [1]. Evaporation in this region not only acts as a main way for exchanges of mass and energy between soil and atmosphere but also an important inducement for the continual migration of soluble salts to soil surface, with a probable result seriously concerned in agriculture, i.e., soil salinization [2, 3]. Now in addition to inducing the above problem, evaporation also answers questions obviously not unrelated but which provide a novel view of the inducement of instability of loess slopes. Evidences were found when interpreting such problems that soluble salts in the soil, after repeated crystallization, dissolution, and recrystallization, were probably enriched at the foot of natural or excavated loess slopes, further leading to the deterioration of engineering performance of the loess [4–7]. Two main aspects should be firstly clarified before solving this problem, namely, the evaporation of soil water and the evaporation-induced migration of water and solutes in the soil towards the surface.

For the first, soil evaporation was generally considered as a process during which soil water was released into the atmosphere in the form of vapor through the bare ground, which

is also an important part of the natural water cycle [8, 9]. The amount of water evaporated is a critical index in evaluating the water and energy balance in agriculture and hydrology, such as soil water prediction, water conservancy construction, and crop yield estimation [10, 11]. However, the determination of soil evaporation is a rather difficult problem [12], in that soil atmosphere is a fairly complex system with soil moisture transport from the soil inside to the atmosphere through the bare ground or the plants covered. It relies on both meteorological factors (e.g., solar radiation, atmospheric temperature, atmospheric humidity, and wind speed) and the soil property (e.g., soil structure, water content, and organic matter content), not to mention the interactions of these factors. Therefore, evaporation measurement methodology has always been the core of soil evaporation research. Many experimental methods have been proposed in recent decades [12, 13], e.g., automatic weighing soil lysimeter, soil evaporating pan, soil column test, heat flux device, infrared thermometer, and Bowen ratio method. Besides, some indirect methods were also adopted in estimating soil evaporation, e.g., the Cooper method [14], the zero flux plane (ZFP) method [15], the modified Fox model [16], the aerodynamic model [17, 18], and the Aydin model [19]. For the second aspect, evaporation induces the migration of soil water and salt to the surface layer, which is to ascertain the coupled transport of heat, water, and solutes in the soil [20, 21]. Soil water transport model is one of the first to be concerned, such as the Darcy's law. As the temperature and solute in pore water were considered, theoretical models gradually developed from a single physical field to the multifield coupling calculation, including water-heat coupled models [22–25], water-solute coupled models [26–29], and heat-water-solute models [30–35].

Saline attack is often seen while urbanization process is progressing [36–37]; experiments proved that sodium sulfate was one of the main constituents of soluble salts that caused salt weathering [4, 6]. Considering the needs of simultaneous identification of soil evaporation and heat, water, and solute transport in the soil, large-sized soil column tests were carried out in a laboratory by using a self-developed device in producing an artificial evaporation environment. Five typical meteorological indexes such as relative humidity, atmospheric temperature, atmospheric pressure, radiation, and wind speed were considered. The frequently encountered Q_3 loess in Loess Plateau, China, was taken to produce soil columns by adding sodium sulfate solutions. The evaporation and coupled transport of heat, water, and solute of the soil were both investigated in closed and open systems.

2. Experiment Program

2.1. Materials and Specimen Preparation. The loess samples were taken from a foundation pit in Lianhu District of Xi'an, with a depth of 8–10 m, which can be classified as the late Pleistocene (Q_3) loess. Following the standard for soil test method GB/T50123-1999, the physical indexes for the taken loess samples were determined while the ion types and contents were determined by ion chromatograph and titration (Table 1). As easily noticed from the measured data, both SO_4^{2-} and Na^+ constitute the majority of the ions identified, with ion contents equal to 0.0080% and 0.0062%, respectively. Thus, the anhydrous sodium sulfate was used in preparing solutions at a target salt content. According to the specimen size, water content, and dry density required by the test, the weight of the slurry was first calculated. The soil samples were air-dried in the laboratory and ground to remove debris such as plant roots and gravel. After sieving by a 2 mm standard geotechnical sieve, the soil at a target weight was put into a storage box to spread it out evenly, and then the prepared sodium sulfate solution (Na_2SO_4 solution) was sprinkled on the soil through a watering pot. The target salt content was controlled to be 0.6%. In order to minimize the evaporation of the slurry in the thermostatic laboratory, the storage box was wrapped with plastic film after spraying. Then, the prepared slurry was weighed and was slowly dripped into ionized water or air-dried in a constant temperature environment to reach the target water content of 20%. Samples (about 30 g) at three different positions were selected to determine the water content by oven drying, and the salt content of dried soils was further measured by salt leaching tests. The maximum deviations from the target water and salt contents are ±1% and ±0.05%, respectively. It was then wrapped in a plastic film to reduce evaporation of water. The prepared soils were kept in a closed chamber with constant temperature and moisture for at least 24 hours

Table 1: Characteristic indexes for the tested loess.

Physical index	Value
Specific gravity, G_s	2.70
Dry density, ρ_d (g/cm^3)	1.42
Water content, ω (%)	15.02
Atterberg limits	
Liquid limit, ω_L (%)	34.3
Plastic limit, ω_P (%)	19.6
Plasticity index, I_p	14.7
Particle grading characteristics	
>0.05 mm	5.0%
0.01-0.05 mm	52.0%
0.005-0.01 mm	24.0%
<0.005 mm	19.0%
Initial ion content	**Value**
Anion content (%)	
CO_3^{2-}	0.0000
HCO_3^-	0.0028
Cl^-	0.0038
SO_4^{2-}	0.0080
Total	0.0146
Cation content (%)	
K^+	0.0013
Ca^{2+}	0.0020
Na^+	0.0062
Mg^{2+}	0.0011
Total	0.0106

Table 2: Pan evaporation in Shaanxi province.

Factors considered	Divisions	Pan evaporation (mm)	Coefficient of variance (%)
Different regions	Overall	1503.7	7.5
	Northern Shaanxi	1792.1	6.3
	Weihe Plain	1466.3	9.7
	Southern Shaanxi	1252.7	7.2
Different seasons	Spring	491.7	10.9
	Summer	617.6	10.1
	Autumn	260.2	14.1
	Winter	134.2	13.6

Table 3: Evaporation test conditions.

No.	Availability of external water	Illumination intensity (W/m^2)	Wind speed (m/s)	Evaporation duration (days)
Test 1	Closed system	60	5	0, 2, 5, 10, and 15
Test 2	Closed system	95	10	0, 2, 5, 10, and 15
Test 3	Closed system	140	15	0, 2, 5, 10, and 15
Test 4	Open system	140	15	0, 2, 5, 10, and 15

so that the moisture can be evenly distributed in the soil. Soil samples after curing for 24 hours were compressed slowly in layers into a plexiglass tube according to the target dry density of 1.45 g/cm^3. In addition to the first layer with a filling thickness of 3 cm, the other layers were controlled to be 8 cm in thickness. From Table 1, the sodium sulfate content in the loess taken in situ is far lower than the target value (0.6%), and thus, its influence on the evaporation and coupled transport of heat, water, and solute can be neglected.

2.2. Test Conditions. Before evaporation tests, the meteorological data of Shaanxi province in the past 35 years were collected from local meteorological stations, including pan evaporation, atmospheric temperature, wind speed, and relative humidity. The mean annual pan evaporation (20 cm in diameter) in different regions and the pan evaporation in each season were shown in Table 2. Table 3 lists the four test conditions for evaporation tests determined according to the collected meteorological data. The former three were carried out in a closed system (without availability of external water) while a Mariotte bottle was connected to the bottom of the plexiglass tube to produce an open system during evaporation testing. The meteorological indexes inside the test device for evaporation were live monitored by high-precision transducers, including atmospheric temperature, relative humidity, radiation, atmospheric pressure, and wind speed. Besides, after reaching a target evaporation duration (2, 5, 10, and 15 days), soil columns were taken out, weighed, and cut into slices. The water and salt contents of each slice were both measured to further analyze the development of temperature profile and the coupled transport of water and solutes.

2.3. Test Device. Figure 1(a) illustrates the self-developed test device for soil evaporation, including four main components such as the overall framework, soil column with plexiglass tube, transducers, and data acquisition system. This device can well produce an evaporation environment close to the natural condition. The overall framework structure, as shown in Figure 1(b), can be divided into two main parts, i.e., the lower and upper parts. The lower part is an angle steel welded frame with 6 mm tempered glasses as the sealing plate, sized at 80 cm × 50 cm × 80 cm (length × width × height). A lifting platform with a Mariotte bottle (Figure 1(c)) was installed on the side wall of the device to supply water to the four soil columns. The upper part is a box made of plexiglass sized at 80 cm × 50 cm × 70 cm (length × width × height). Five round holes with a diameter of 110 mm were drilled at the bottom of the box so that soil columns and comparative water glass for potential evaporation can be well stuck on the holes. Four fluorescent lamps were installed on the top surface of the upper part to provide light source. Fans and wind speed sensors were installed on two opposite sides of the box, and the side plate with wind speed transducers installed is a porous plate for ventilation. The data acquisition system is shown in Figure 1(d), consisting of a data acquisition board and a multichannel board. The transducers for total radiation and wind speed were connected to the data acquisition board. Four temperature transducers and four atmospheric pressure transducers were connected to the multichannel board. The data acquisition board and the multichannel board were, respectively, powered by DC 12 V power supply. The data acquisition board was finally connected to the computer equipped with a data acquisition software, which can set sampling parameters, such as sampling time and storage cycle. The data can also be displayed online for live measurement, and the final data collected will be saved in EXCEL form. As shown in Figure 1(e), four types of transducers were installed, including one total radiation transducer, one wind speed transducer, four atmospheric pressure transducers, and four temperature and humidity transducers. The range and accuracy of these transducers are shown in Figure 1(d). In addition to the wind speed transducer, the other three were bolted to the bottom plate of the upper box. Four sets of atmospheric pressure transducers and four temperature and humidity transducers were, respectively, fixed at a position close to the surface of the soil columns.

Two types of soil column tubes were used in testing, as shown in Figure 2. The first was applied in the closed system with inner and outer diameters equal to 100 and 110 mm (Figure 2(a)). The tube with an overall height of 75 cm was divided into ten sections with the height of each section equal to 8 cm in addition to the first section with a height of 3 cm. Temperature transducers were set in soil column at an interval of 3 cm through the drilled holes in the tube. The joint between the two adjacent sections was flanged, and the bottom was blocked. The soil column tube in the open system (Figure 2(b)), with an overall height of 80 cm, was divided into eleven sections with the first equal to 5 cm. A water supply valve connected to the Mariotte bottle was set at the bottom of the water chamber while the rest was the same as the soil column tube with the availability of external water.

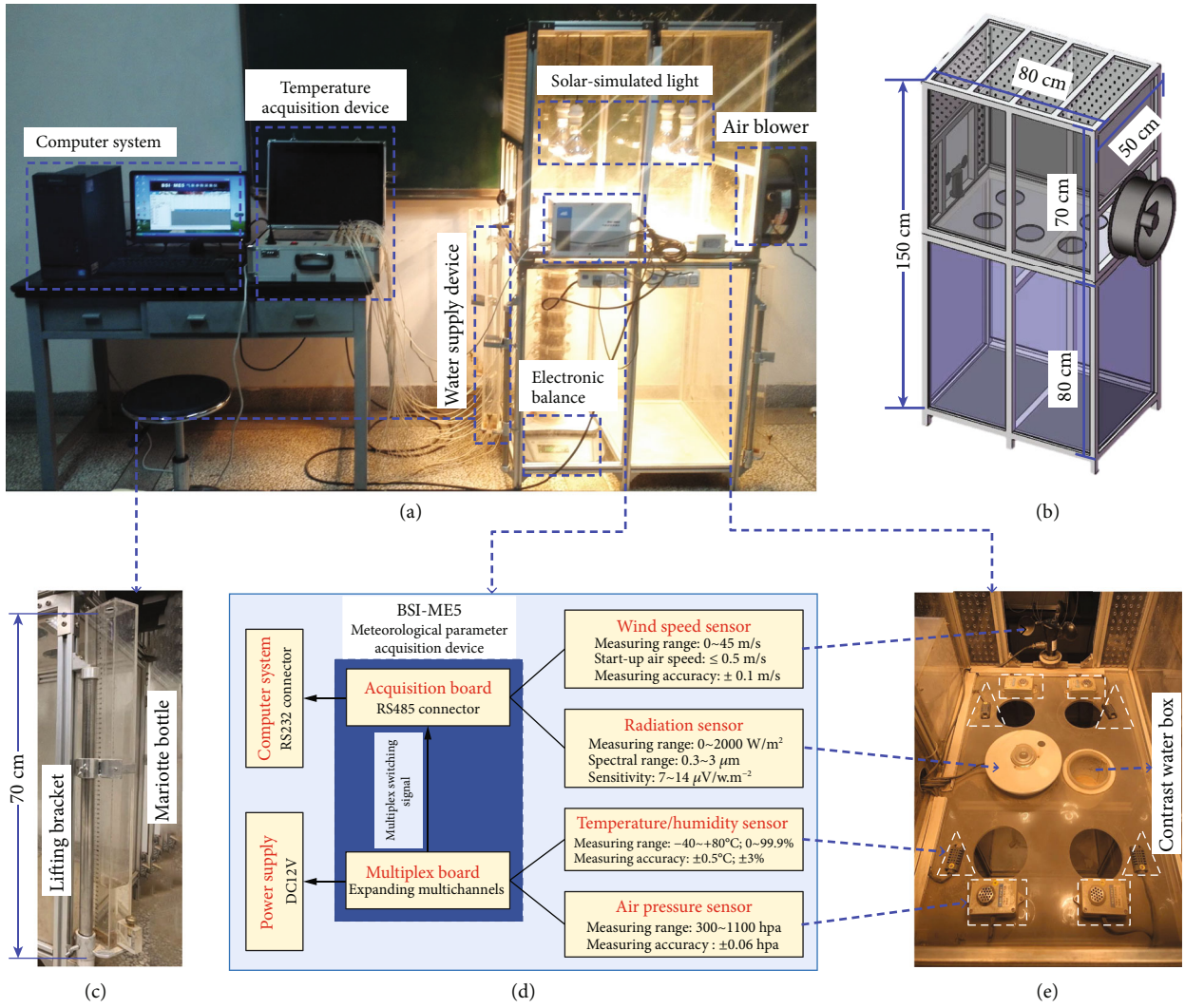

Figure 1: Test device: (a) overall view; (b) dimensions of the frame; (c) water supply device; (d) data acquisition system; (e) transducers.

2.4. Test Method. The prepared soil column was first weighed and placed in the test device. A group of four soil columns was tested each time. The infrared lamp and the fan were turned on, and the measurement software was connected during the evaporation test. The amount of evaporation in the comparative water glass was monitored daily, regarded as the potential evaporation. Evaporation was stopped after continuous evaporation for 0, 2, 5, 10, and 15 days, respectively. The temperature, relative humidity, atmospheric pressure, radiation intensity, and wind speed at the evaporation surface were collected by the acquisition software. Temperatures were measured by transducers at preset positions in soil columns. Then, soil columns were taken out, weighed, and cut. From top to bottom, soil columns were cut every 3 cm. Soil samples were taken to measure the water content by oven drying, while the ion contents by ion chromatography. The difference between the masses before and after evaporation of the soil column is actually the amount of evaporation. The above test procedure was repeated to obtain results under four different conditions. The water level in the Mariotte bottle is equal to the base of the soil column, i.e., in a nonpressure water supply mode.

3. Results and Analysis

3.1. Evaporation of Soil Columns

3.1.1. Analysis of Meteorological Factors during Testing. Figure 3(a) gives the relative humidity of air on soil surface under four test conditions. In the closed system, the three curves all exhibit progressive decline over time. At higher radiation and wind speed, the relative humidity increases. This may result from the fact that a higher rate of evaporation occurs in the initial stage but the amount at each test condition is still limited. The phenomenon that the saturated vapor pressure grows over time also accounts for this trend. As the evaporation continues, the evaporation rate decreases, and the molecular weight of the water that escapes into the air decreases rapidly. Therefore, the relative humidity of air in the device shows a decline. The higher the radiation intensity, the greater the saturated water vapor pressure, resulting in lower relative humidity. However, the evaporation of the soil column also grows at higher radiation and wind speed, with more water molecules escaping into the air and further

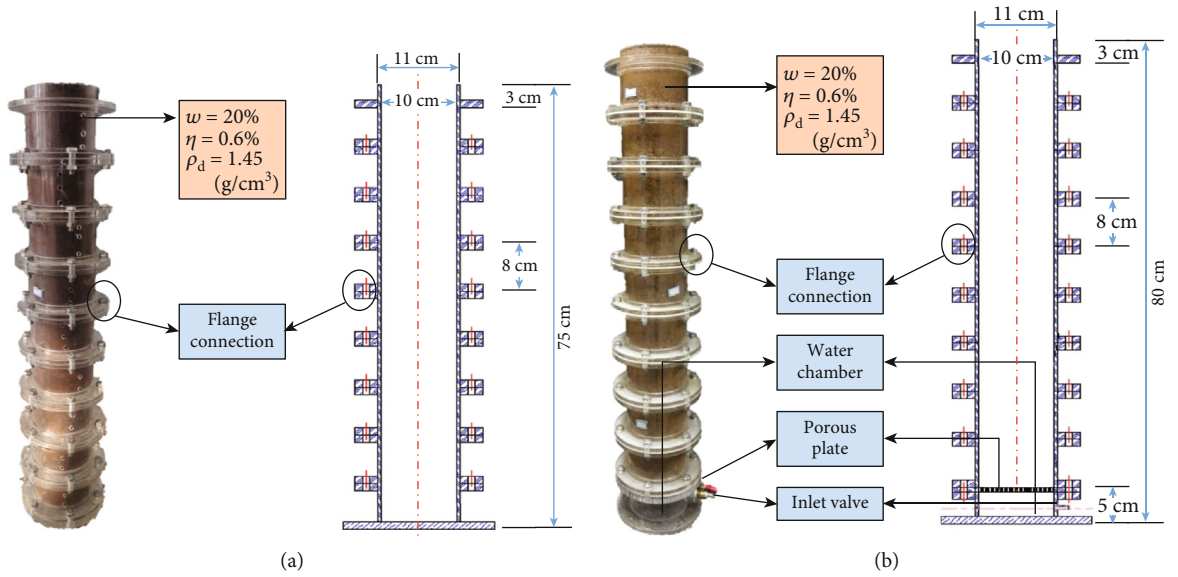

Figure 2: Soil columns for evaporation tests: (a) in the closed system; (b) in the open system.

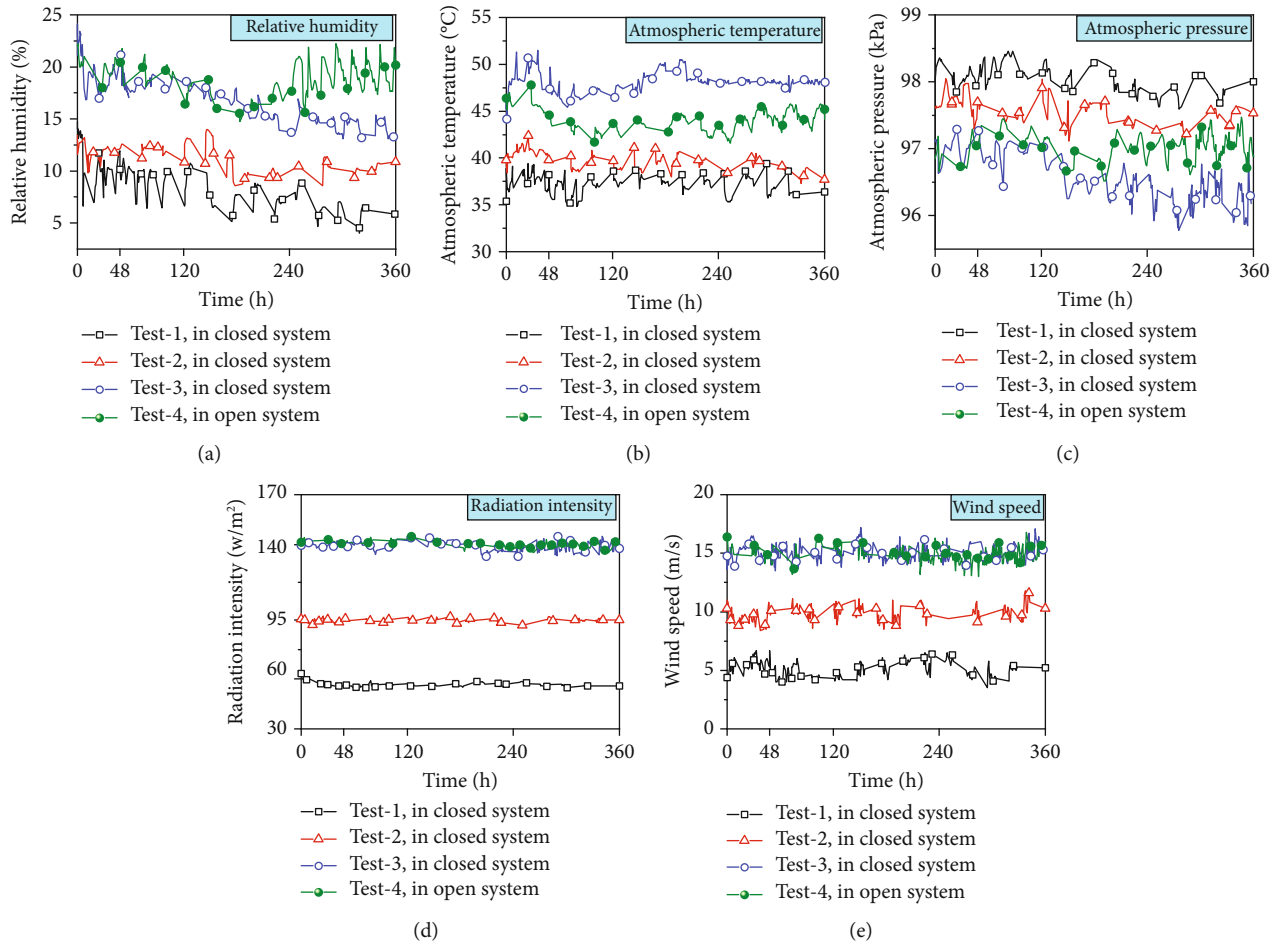

Figure 3: Meteorological factors during evaporation process.

a greater water vapor pressure. The relative humidity instead increases. The overall relative humidity in the device depends on the coupled effect of the two simultaneous processes. In the open system, compared with Test 3, the external water supply is not pronounced due to the larger depth of soil column and hysteresis effect of water migration. The evaporation

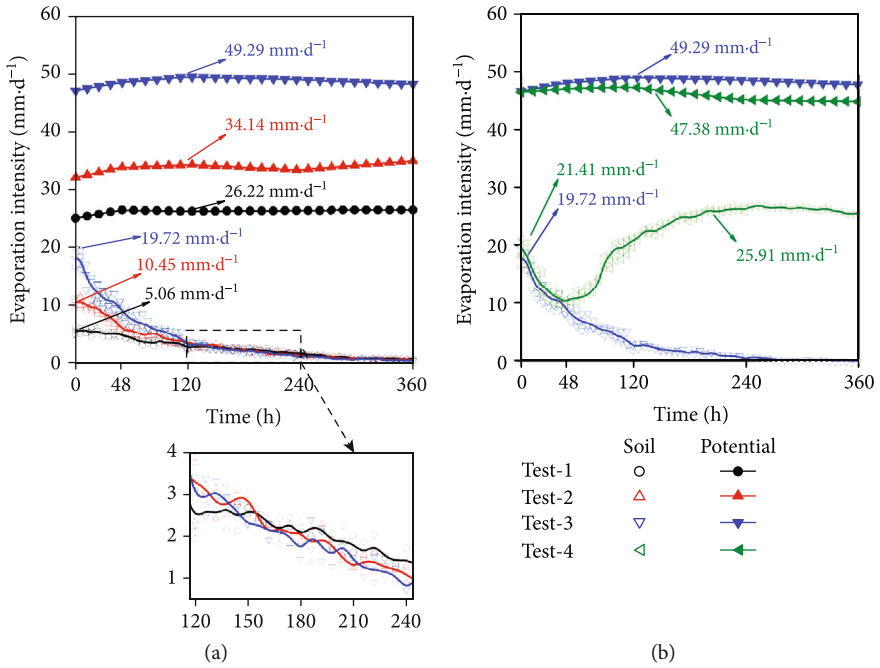

Figure 4: Evaporation intensity: (a) in the closed system; (b) comparison between closed and open systems.

is mainly controlled by meteorological factors, and the two curves are basically consistent in the early stage. In the late stage, since the atmospheric temperature is basically constant, the saturated vapor pressure manifests little change. The moisture entering the air increases as more water was supplied through the Mariotte bottle. In this case, the relative humidity tends to stabilize with insignificant fluctuation.

Figure 3(b) shows the atmospheric temperature on soil surface over time. The higher the solar radiation, the higher the atmospheric temperature and ground temperature. The evaporation surface will also be heated. A higher water vapor pressure difference will be produced, thus accelerating the soil evaporation. In the closed system, the air was rapidly heated in the early stage of evaporation and the temperature approaches to a stable value which grows positively with radiation intensity. However, due to the day-night temperature difference and instrument measurement error, small fluctuations appear in the curves. As the external water is available (in the open system), the atmospheric temperature is lower than that in the closed system in that the higher evaporation capacity will absorb more energy at a given constant heat source.

Figure 3(c) presents the atmospheric pressure on the surface of soil columns. In the closed system, the three curves all exhibit decreasing trend over time but the magnitude declines at a higher radiation intensity. The changes in the atmospheric pressure strongly depend on the specified environment. The higher the radiation intensity, the higher the air temperature on the surface of the soil. The higher wind speed will cause a more active molecular motion, and thus, air density in the unit square will be reduced, and the atmospheric pressure decreases naturally. In the late stage, the rate of evaporation decreases with less vapor entering the air, and the pressure drops. Comparing the curves in closed and open systems (Test 3 and Test 4), the meteorological conditions

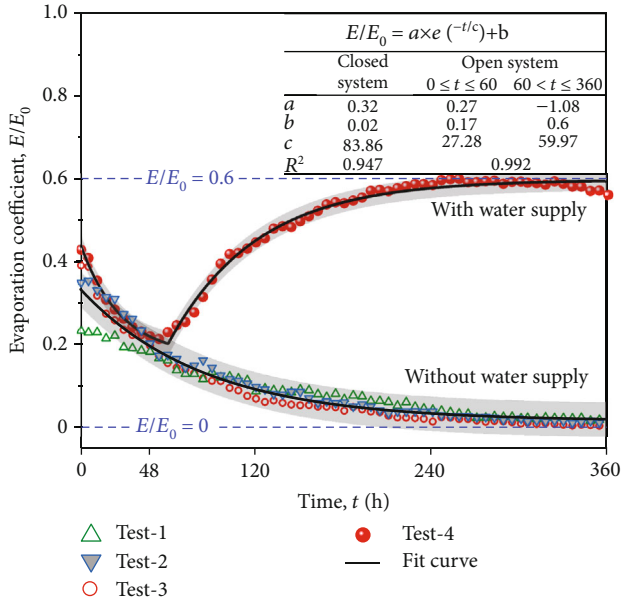

Figure 5: Evaporation coefficient under considered test conditions.

play a dominant role in the early stage of evaporation, and the two curves are basically the same. But beyond this stage, the soil column continuously evaporates into the air, resulting in higher pressures in the open system. The radiation intensity and wind speed shown in Figures 3(d) and 3(e) vary within a narrow range as the evaporation proceeds and in general stabilize at the preset standards. The above analysis proves that the meteorological conditions produced in the test device can well meet the requirements of soil evaporation tests.

3.1.2. Evaporation Intensity. Figure 4(a) illustrates the evaporation intensities of water glass and soil columns at the three

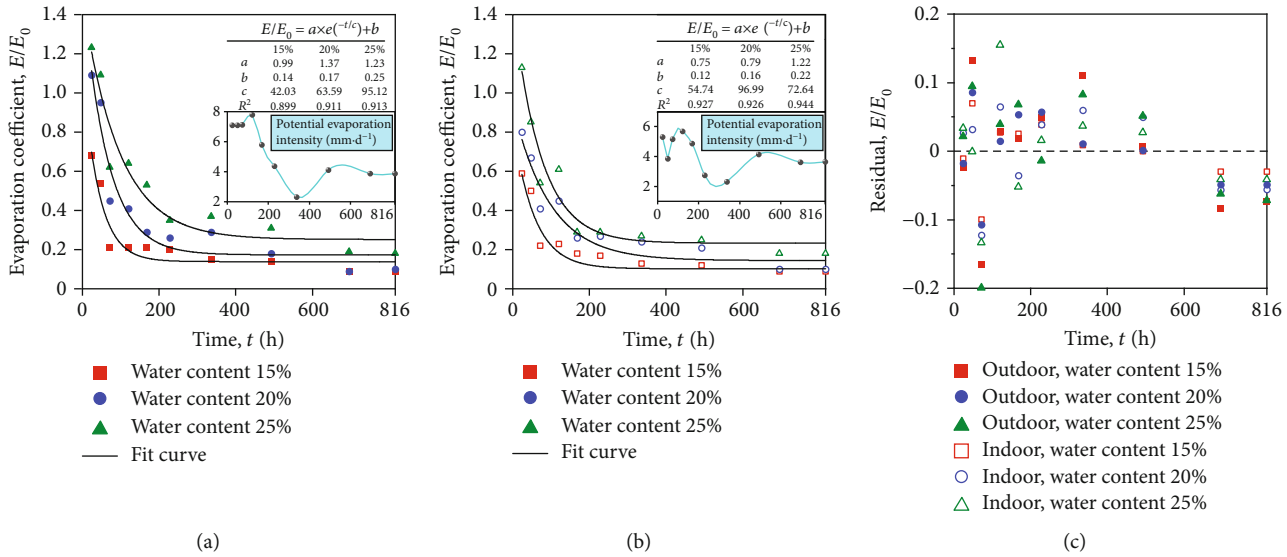

Figure 6: Fit results for evaporation of salt-free loess: (a) laboratory tests; (b) outdoor tests; (c) RMSE.

conditions in the closed system. The evaporation intensities, at the three conditions, exhibit roughly identical variations over time, which could be classified into three typical stages. In the first stage that corresponds to the early stage of evaporation, the rate of evaporation is relatively higher than the other two stages. The second stage followed continues with evaporation rate decreasing rapidly. In the third stage, the evaporation rate approaches to zero and the curves at the three test conditions (Test 1, Test 2, and Test 3) tend to be overlapped.

The evaporation of water, macroscopically, refers to the process of gradually changing water from liquid to vapor. While from a micro perspective, the evaporation of water is actually a process in which water molecules overcome the intermolecular attraction between liquids under kinetic energy and escape from the liquid surface to the atmosphere. As the evaporation environment is initially produced, the resistance that water molecules need to overcome to escape to the atmosphere is the smallest, so the evaporation rate is the highest in the first stage of evaporation. Compared with different test conditions, the evaporation rate grows at higher radiation and wind speed. The wind keeps the air close to the surface of the soil continuously disturbed and takes away the air with a higher vapor pressure and replaces it with dry air to accelerate the evaporation process. The greater the wind speed, the stronger the evaporation. As the evaporation proceeds, the evaporation rate drops sharply with a slight rise in the evaporation curve, which may result from two main aspects. The suction in the soil continues to increase with the evaporation, which enhances the effect of inhibiting the escape of water molecules (or water retention capacity). Suction also causes the soil to shrink, i.e., the particle space and pore size, resulting in a decrease in the water permeability. Evaporation always starts from the surface of the soil and gradually develops into the interior of the soil column, firstly evaporating gravity water, followed by capillary and weakly bound water, and strong bound water generally does not

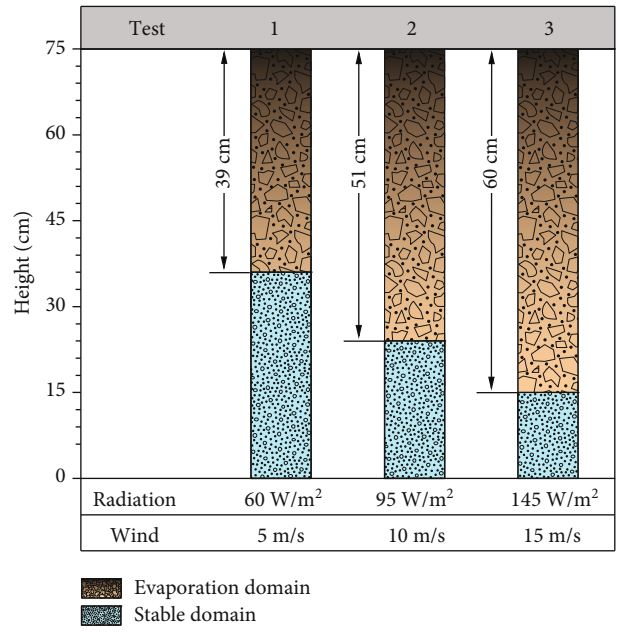

Figure 7: Evaporation-affected domain in soil columns in the closed system.

participate in evaporation. The rate of evaporation tends to a small constant value when the test condition is basically stable. In the later stage, less soil water is available for evaporation, and the connectivity of pore water decreases with capillary action weakened. In addition, water is mainly distributed in some relatively small pores, which are strongly constrained by soil particles. In this case, the upward migration of soil water driven by the difference of water content in soil profile (or the gradient of matric potential between upper and lower soil layers) is limited. In the meanwhile, more pore gases exist in the interpenetrated soil pores and the evaporation of water inside the soil is gradually dominated by water

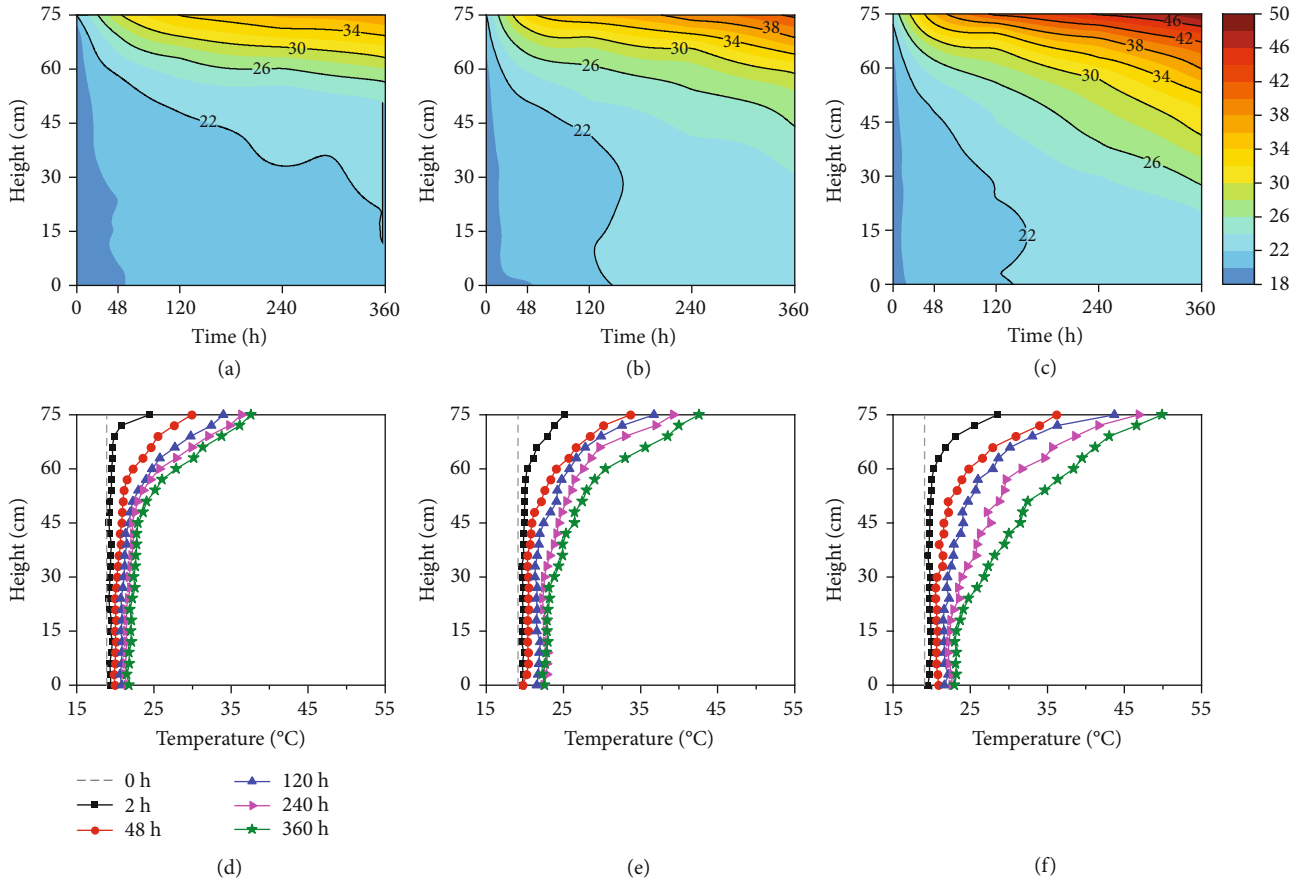

FIGURE 8: Temperature profiles in soil columns during evaporation: (a) Test 1, time-history curve; (b) Test 2, time-history curve; (c) Test 3, time-history curve; (d) Test 1, profile; (e) Test 2, profile; (f) Test 3, profile.

vapor diffusion. The evaporation rate tends to zero, indicating a stable evaporation process.

The cumulative evaporation and evaporation rate of soil columns in closed and open systems (Test 3 and Test 4), at a radiation intensity of 140 W/m^2 and a wind speed of 15 m/s, were presented in Figure 4(b). The curves representing the relationship between evaporation intensity and test duration in closed and open systems (Test 3 and Test 4) show limited difference within a duration of 0–48 hours (the early stage of evaporation). The evaporation of soil water is concentrated only in the upper part, and most of the water supply for evaporation is also derived from the interior of the soil, so the curves in this stage are almost the same. It also implies the hysteresis characteristics of the external water supply, especially in a nonpressure supply mode. Beyond this duration, the cumulative evaporation of the soil column in the open system is higher than that in the closed system. However, the potential evaporation intensity in the closed system is a little higher.

With the continuing evaporation, the evaporation surface in the closed system moves downwards. The suction of the soil grows significantly, enhancing the constraint of water molecules by soil particles, and the water available for evaporation is reduced since most of the weakly bound water has been evaporated. It should also be noted that the connectivity of pore water is disturbed, with the water in the lower part to migrate to the evaporation surface prolonged. As a result, the evaporation rate decreases sharply and the amount of water evaporated is insignificantly increased, while in the open system the growing suction in the soil causes a higher gradient of matric potential in soil column as the evaporation proceeds. In the early stage of evaporation, even if the change of evaporation intensity is close to that in the closed system, the external water was continuously absorbed by the soil column, leading to a higher rate of water migration towards the evaporation surface. Correspondingly, the slope of the curve representing the evaporation intensity over time rises sharply. In the late stage, the evaporation of water inside the soil gradually takes the water vapor diffusion as the dominant form, and the evaporation rate is limited in the closed system, while in the open system the water evaporated from the soil can be well replenished, manifesting a stable evaporation rate.

3.1.3. Evaporation Coefficient and Evaporation-Affected Domain. The evaporation intensity mainly depends on two factors, i.e., (i) the meteorological factors such as radiation and wind speed, which determine the energy required by initiating and keeping up the evaporation and the diffusion process of surface water vapor to the atmosphere, and (ii) the water supply capacity of the soil that further affects the

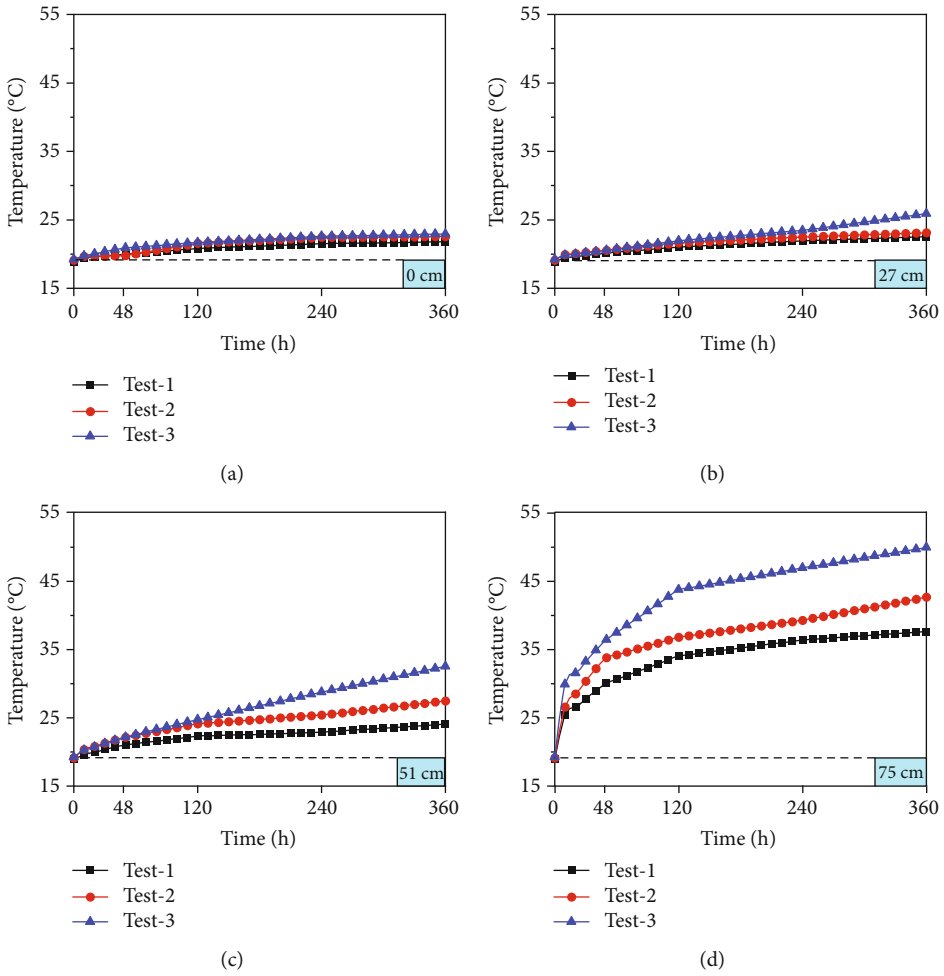

Figure 9: Variation of temperature at a specific depth.

profile of water in the soil. In order to study the mechanism of soil water transport, the ratio of evaporation intensity of soil column to potential evaporation intensity is defined as evaporation coefficient. Since the potential evaporation intensity is a comprehensive reflection of the amount of radiation, wind speed, etc., the evaporation coefficient can well characterize the water supply capacity inside the soil, which can be written as

$$\frac{E}{E_0} = a \cdot \exp\left(-\frac{t}{c}\right) + b, \tag{1}$$

where E (mm/d) is the evaporation intensity of soil column; E_0 (mm/d) is the potential evaporation intensity; t (h) is the evaporation duration; a, b, and c are fitted parameters.

Figure 5 presents the fitted results of the evaporation coefficient of soil columns under four considered conditions. In the closed system, although the evaporation intensity E of the soil column differs greatly from the potential evaporation intensity E_0, the evaporation coefficient E/E_0 shows limited change over time. In the early stage, soil evaporation is dominated by environmental factors. The tested loess in unsaturated state exhibits an extremely short duration, with a lower evaporation coefficient, approaching to zero as the evaporation proceeds. However, the evaporation coefficient for soil columns in the open system varies significantly over time, except that in the early stage of evaporation. Like the curves in the closed system, the coefficient of evaporation within this stage in the open system is primarily controlled by the preset meteorological conditions. Thus, the curve in the open system is very close to but a little higher than that in the closed system in this stage. After this stage, the amount of the water available for evaporation grows due to the sufficient supply of water from the Mariotte bottle. The evaporation coefficient rises rapidly and exceeds the initial value just as the evaporation of soil columns begins. However, it lies in the range of 0-1, i.e., $E/E_0 = 0.6$, rather than a constant close to 1, even though the evaporation was prolonged to 360 h. It can be inferred that the water in the phreatic surface directly evaporates in a free mode while that in soil columns has to pass through complicated paths formed in pore structure to the atmosphere, during which large amounts of energy will be consumed to overcome the resistance to evaporation. Moreover, the solutes in the lower part are transported to the evaporating front with water, resulting in a high salt

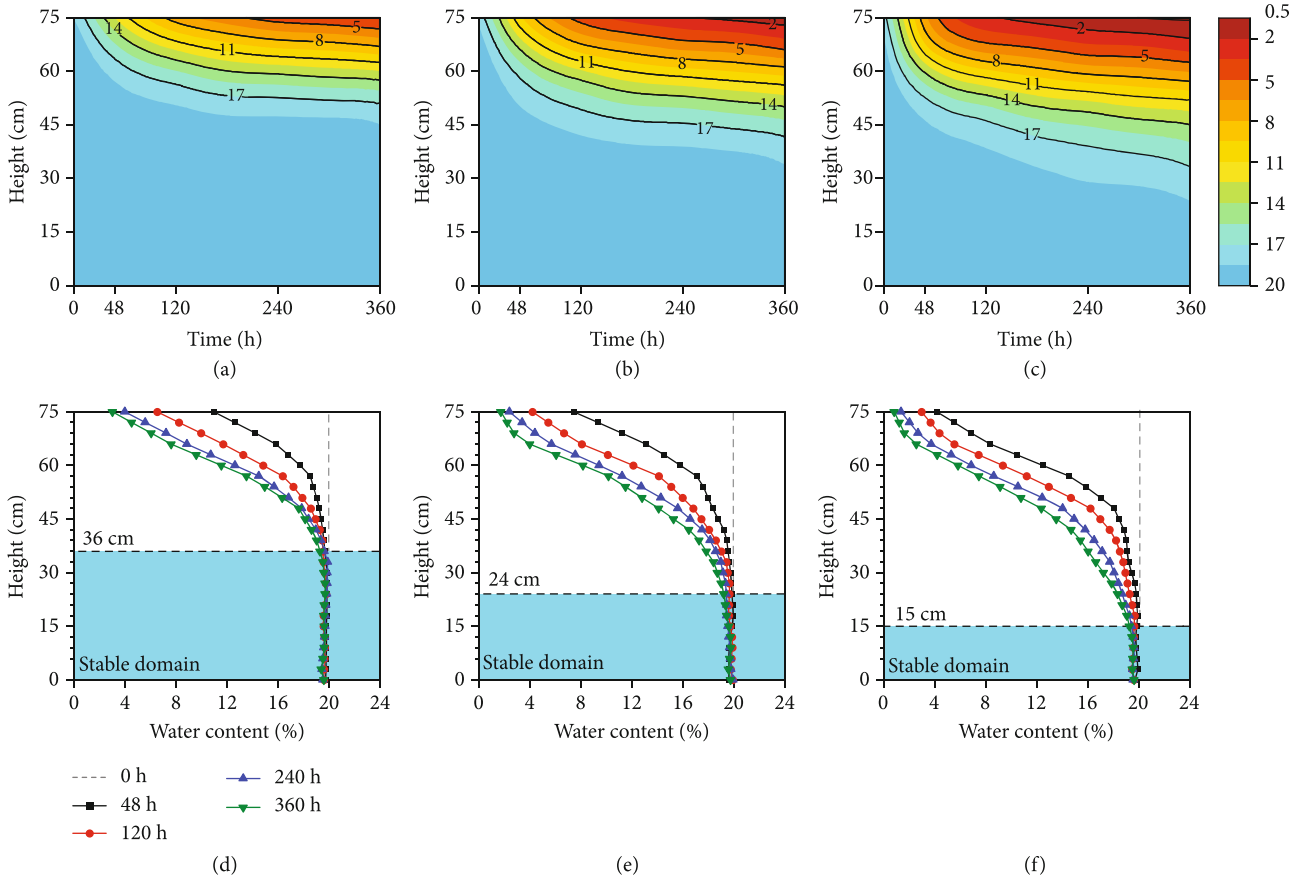

FIGURE 10: Water profiles in soil columns during evaporation: (a) Test 1, time-history curve; (b) Test 2, time-history curve; (c) Test 3, time-history curve; (d) Test 1, profile; (e) Test 2, profile; (f) Test 3, profile.

concentration in this domain, called the salt shell. The energy required for soil water to evaporate into the air is further increased due to the formation of the salt shell. The two processes cause the evaporation coefficient curve to stabilize near a certain value, and it is worth noting that there is a slight decline in the later stage of the measured curve.

In order to verify the rationality of the above empirical equation, the evaporation coefficients, as listed in the literature [38], for Xi'an loess determined in the laboratory and outdoors in the closed system were fitted (Figure 6). Note that the loess samples in the same area were tested by Chen [38] and the influence of the initial salt content is not considered. Clearly as it proves in Figures 6(a) and 6(b), the data points lie close to the fitted curves, with regression coefficients higher than 0.90 and the root-mean-square error of -0.2–0.2 (Figure 6(c)), indicating a good fitting effect of the equation. For the changes in the water profile in the closed system, the area where the water content varies insignificantly is defined as the stable domain while the rest is the evaporation-affected domain. Figure 7 presents the evaporation-affected domain in soil columns under the considered test conditions. As the radiation intensity and wind speed increase, the depth of the evaporation-affected domain grows and that of the stable domain decreases. Correspondingly, the evaporation-affected domains of soil columns in the closed system, identified as Test 1, Test 2, and Test 3, are 39, 51, and 60 cm in depth.

3.2. Profiles of Temperature, Water, and Solute in the Closed System

3.2.1. Temperature Profile. The time-history curves under the considered test conditions, as presented in Figures 8(a)–8(c), prove that the temperatures in soil columns vary in basically the same mode over time and the highest temperature appears at soil surface. Within a certain range beneath the surface, a pronounced change in soil temperature was found from test data. This range also enlarges positively with radiation intensity and wind speed. This may correspond to the evaporation-affected domain mentioned in the previous section. In the meanwhile, an insignificant change in soil temperature occurs at the bottom of soil columns. This may result from the fact that the surface of the soil column is the closest to the heat source, and soil temperature is higher when a heat source with larger intensity was applied during testing, especially for the domain close to the heat source. A larger range influenced by the heat source can also be noted from time-history curves. Figures 8(d)–8(f) illustrate the temperature profiles of soil columns at various evaporation durations. At the beginning, the temperature of the surface

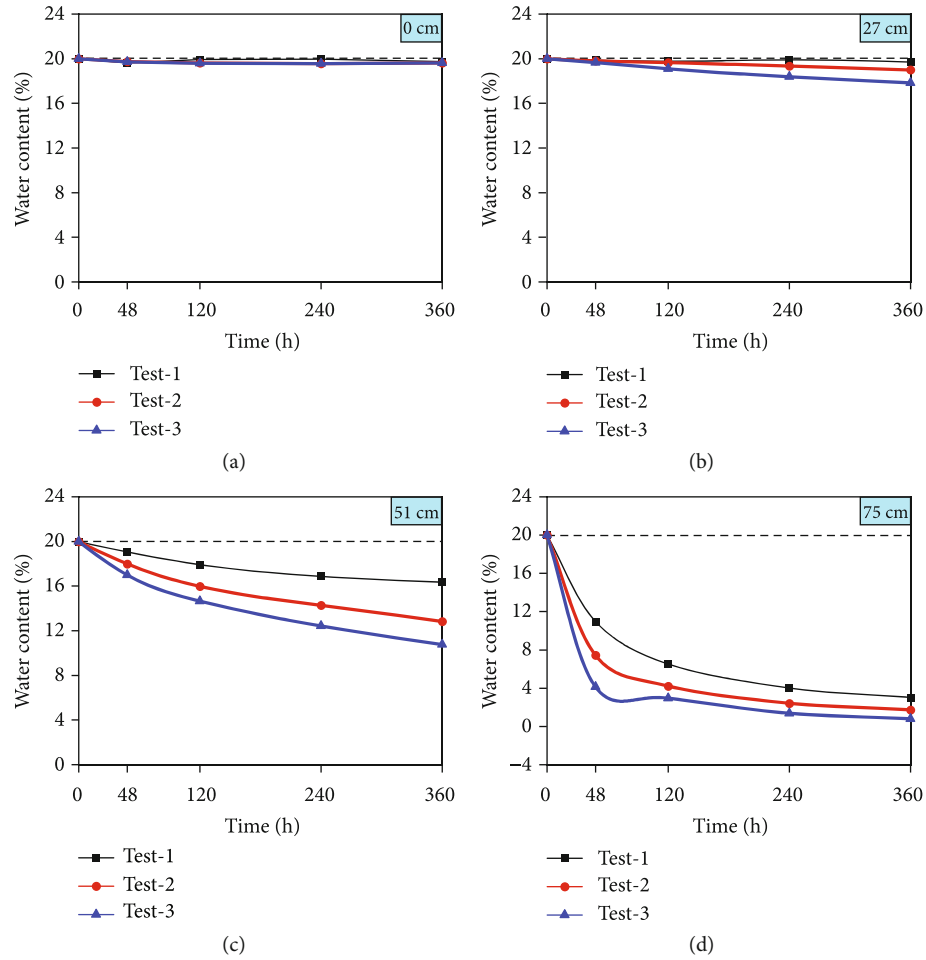

Figure 11: Variations of water content at a specific depth.

rises rapidly and that inside the soil also grows over time. It is worth noting that the part near the bottom of the soil is weakly affected by evaporation, so the temperature variation is limited, and the length of the part decreases at higher radiation intensity and wind speed.

Variations of soil temperature at a specific depth, as given in Figure 9, indicate that under the three test conditions (Test 1, Test 2, and Test 3), the highest temperature occurs in Test 3 with higher radiation intensity and wind speed. Note that the radiation and wind speed are the lowest in Test 1 and a slight change in temperature can be observed at a height of 51 cm, where, however, a greater rise appears in Test 3. As can be inferred, the greater the radiation intensity, the greater the depth of its influence on the temperature profile. Besides, the temperature at the soil surface is obviously higher than that at the bottom, which is closely correlated with the preset heat transfer path from top to bottom. Even though the evaporation of soil columns absorbs heat, the amount that induces soil column heating is much greater than the heat loss. As evaporation goes on, the evaporation surface moves continuously downwards, and the topsoil is continuously heated. Correspondingly, as the evaporation continues, the surface temperature keeps rising.

3.2.2. Water Profile. Figures 10(a)–10(c) show the time-history curves of the water profile under different test conditions. A stable domain, where the water content of the soil in each monitored layer changes insignificantly, can be easily noted from the profiles of water content in soil column at each test condition. The height of the stable domain is closely related to the evaporation condition, manifesting as a narrowed range when the radiation intensity and wind speed increase, e.g., the stable domain identified from Test 1 to Test 3. The changes in water content of the soil are limited, as easily found from the overlapped curves in this domain. In the upper evaporation zone, the water content of the soil decreases rapidly as the height increases, and the water content at the surface of soil column is the lowest. As higher radiation intensity and wind speed are applied, e.g., Test 3, this lower limit further declines. Figures 10(d)–10(f) show the distribution of water along the soil column after various evaporation durations. The curves at each test condition in the closed system present similar variations with test duration. The curves are located to the left of the line representing the initial water content. The minimum value exists near the soil surface, below which a substantial change occurs in the evaporation-affected domain. When

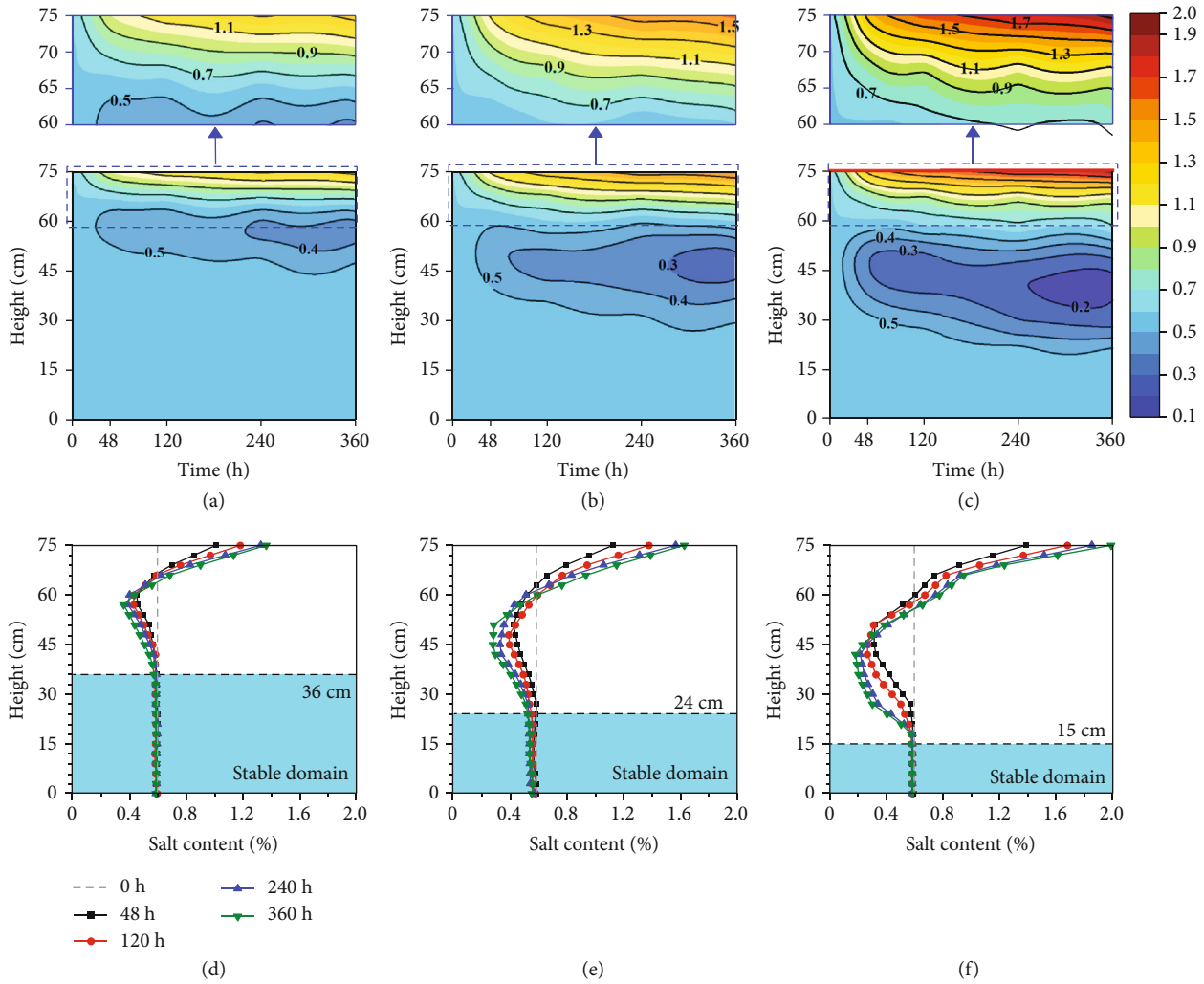

Figure 12: Salinity profiles in soil columns during evaporation: (a) Test 1, time-history curve; (b) Test 2, time-history curve; (c) Test 3, time-history curve; (d) Test 1, profile; (e) Test 2, profile; (f) Test 3, profile.

the evaporation surface reaches a certain position, the water profile is basically stable, as shown in the blue area of Figures 10(d)–10(f).

Figure 11 represents the relationship between water content of the soil and evaporation duration at a specific depth. Under the three test conditions, lower gradients of matric potential are formed in the stable domain, resulting in a lower driving force for soil water migration and thus causes limited amount of water migrated towards the evaporation surface. Close to the surface of the soil column, the curve changes drastically. The curve lies in a lower position in the figure at greater radiation intensity and wind speed, which is closely related to the amount of water consumed during evaporation. Also, the curves exhibit consistent changes at the considered test conditions. The gradient of matric potential is lower in the stable domain, causing a limited amount of migrated water and a lower amplitude of variation influenced by such a weak driving force for the migration of soil water. In the above domain affected by evaporation, a substantial decrease in the water content occurs at the soil surface, far lower than that at a depth of 51 cm. During the initial evaporation period of 0–48 h, the soil is heated rapidly, and the energy for water vaporization is enough. A higher rate of evaporation is satisfied at a higher vapor pressure gradient at the rustic interface, with pronounced water consumption. After 48 hours, large amounts of water loss occur at the surface of the soil column, while evaporation always evaporates gravity water first, followed by capillary and weakly bound water, and finally the strong bonding water. Therefore, the rate of evaporation will inevitably decrease at a specified test condition, corresponding to the limited variation in the middle and late evaporation stages.

3.2.3. Salinity Profile. Figures 12(a)–12(c) show the time-history curves of the salinity profiles under the three test conditions. The solutes were accumulated in a domain with the height ranging from 60 to 75 cm in the upper part of the soil column. The amount of evaporation increases at higher radiation intensity and wind speed, and the content

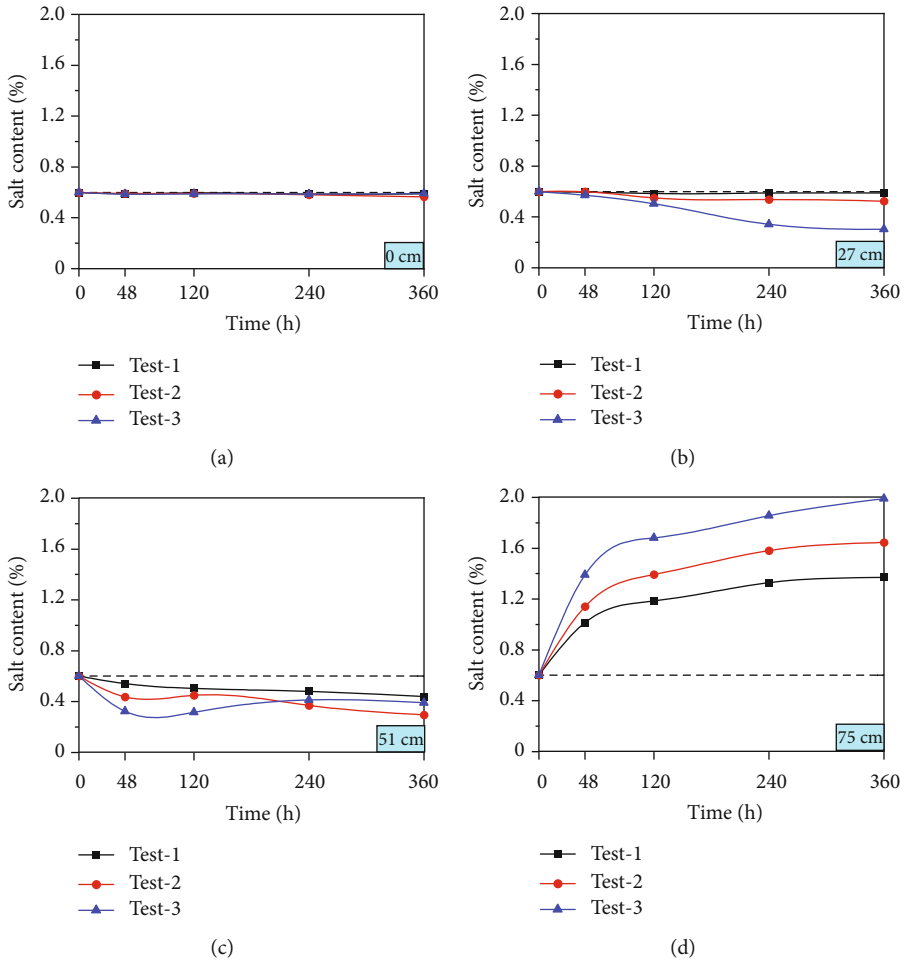

Figure 13: Variations of salt content at a specific depth.

of the salt accumulated in this domain increases as well. On the contrary, the minimum value in the lower part (0–60 cm in height) of the soil column declines simultaneously and appears in a domain that moves downwards with the test condition (from Test 1 to Test 3). Figures 12(d)–12(f) show the variation of the salt profile with evaporation duration under different test conditions. Similar changes in the profile can be easily noted from the measured curves under the considered conditions, i.e., the surface aggregates the most salt, and the content declines at a higher position in the soil column with a visibly minimum value at a certain position between the stable domain and the upper salt-rich area (60–75 cm). In the stable domain, the salt content grows again and then gradually stabilizes. The salt content of the soil surface grows positively with the test condition, more specifically, at higher radiation intensity and wind speed, implying an obvious accumulation of soluble salts. This can be attributed to the coupled transport of water and salt in the soil induced by the continuous evaporation. In other words, the water in the soil acts as a carrier of the migrated salts. It is worth noting that in the stable domain of the water profile, the content of soluble salts almost maintains a stable state. This also reflects the close correlation between water and salt migration.

Figure 13 shows the changes in salt contents of the soil over time, at four considered positions of the soil columns, i.e., 0, 27, 51, and 75 cm. The migration of salt in the soil is accompanied by the water movement. In the stable domain, a limited amount of water migrates, so the salt content hardly changes. At the surface of the soil column, at the beginning of evaporation, the soil is heated rapidly, and the energy for water vaporization is sufficiently provided by the test device. At a higher vapor pressure gradient at the rustic interface, more water participates in the evaporation process with a higher rate, and the rate and amount of salt migrated are pronounced, manifesting as a rapid rise of the curves. Comparing the test results at the three considered conditions, the amount of evaporation grows simultaneously with that of the soluble salt; correspondingly, the curves move upwards in the figure. After 48 h, the curve rises slowly because the evaporation always evaporates gravity water first, followed by capillary and weakly bound water, and finally strong bound water, and the water supply from the lower part is seriously insufficient. Thus, the solutes hardly migrate in this case. This can also explain why such gentle changes were noted in the profiles of water and salt in the stable domain. Taking the test data at a depth of 51 cm in Test 3 as an example, the salt content will decrease as the water migrates

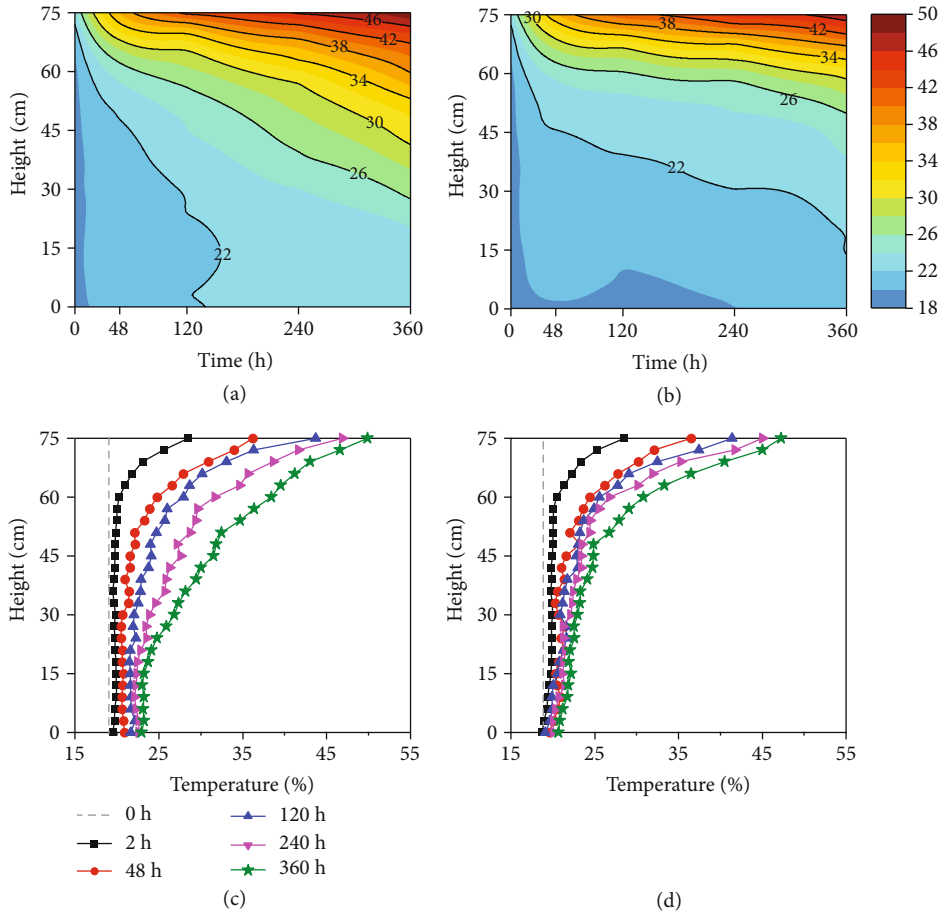

Figure 14: Temperature profiles in closed and open systems: (a) time-history curve in the closed system; (b) time-history curve in the open system; (c) profile in the closed system; (d) profile in the open system.

upward, accompanied by the transport of soluble salts in the initial stage of evaporation. The evaporation intensity is rapidly weakened over time, and the content of the salt migrated from the lower part increases slightly.

3.3. Comparison of Heat, Water, and Solute Transport in Closed and Open Systems

3.3.1. Temperature Profile. The time-history curves of temperature profiles in closed and open systems, as shown in Figures 14(a) and 14(b), manifest similar variations with height, i.e., soil temperature grows over time with the maximum value existing at the surface and the gradient of temperature in soil columns grows at a higher position. The difference lies in the change in soil temperature in the lower part close to the bottom of soil columns. A more pronounced increase can be observed in the closed system, compared with that in the open system, due to the heat consumption induced by the continual water supply from the Mariotte bottle. Figures 14(c) and 14(d) present the comparison of temperature profiles in the two systems. Compared with that in the closed system, a gentle change in soil temperature can be noted in the open system, especially within the lower half of the soil column.

The temperature at a specific depth in the open system is higher than that in the closed system, as shown in Figure 15. Besides, a larger difference exists at the top and bottom of the soil column while in the central part the two curves tend to be overlapped. This phenomenon probably results from two main aspects. The first is the requirement of more heat of vaporization during evaporation due to the continuous supply of external water that is in a relatively lower temperature. The second is the growing heat capacity of the soil as more water is incorporated. It can be deduced that at given radiation intensity and wind speed, the temperature in the closed system is likely to exceed that in the open system.

3.3.2. Water Profile. Time-history curves for the moisture field of soil columns in closed and open systems were shown in Figures 16(a) and 16(b). During evaporation, the contour lines, unlike those in the closed system, have not shown obviously monotonic changes over time. The isolines in the upper part of the soil column move downwards with time in the initial 48 hours but tend to rise slightly afterwards until the curves almost stabilize after 240 h. While those in the lower half of the soil column significantly increase with an attenuated increment, until a duration of 240 h, beyond which, the water content only varies within a narrow range ($\Delta w < 2\%$). Figures 16(c) and 16(d) describe the profiles of water content of the soil columns in closed and open systems. As noticed from the figure, the water content of the soil at a

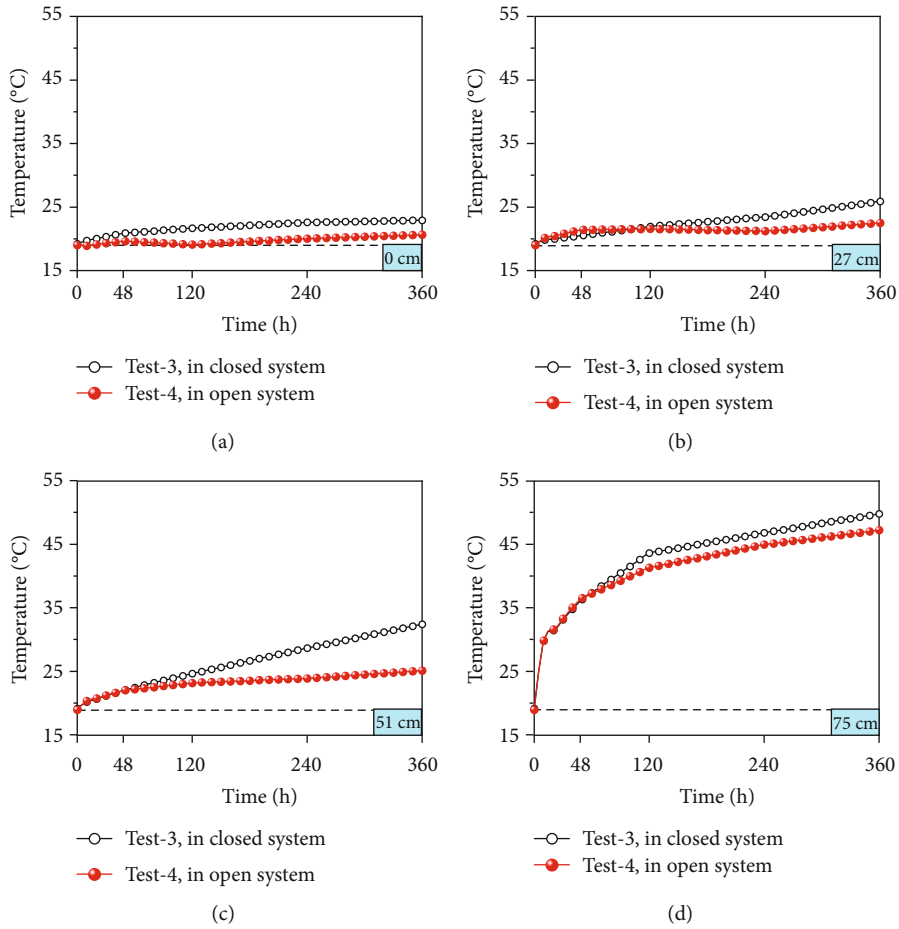

Figure 15: Variations of temperature at a specific position in closed and open systems.

specific position in the open system varies significantly compared with that in the closed system. In the early stage, the external water supply has not shown such an obvious effect on the water profile due to the hysteresis behavior that the supplied water cannot immediately replenish the water loss during evaporation. Meteorological factors such as radiation intensity and wind speed dominate this stage, resulting in similar curve patterns in closed and open systems. The evaporation front moves towards the interior of the soil which is further dehydrated. The matric suction gradient between the upper and lower layers increases, producing a potential driving force for water migration. In addition, the increase in matric suction has a negative effect on evaporation, and the shrinkage of the soil pores and the enhanced bounding of water molecules both lead to a lower permeability of the soil. Overall, the water in the lower part of the soil column migrates upwards at a higher gradient of matric suction. The evaporating surface moves upwards as the evaporation proceeds until a relatively stable stage is reached. In this stage, the gradient of matric suction stabilizes, manifesting as the parallel curves in the right part of the figure (240–360 h).

Variations of water content at a specific position of the soil column, shown in Figure 17, prove that little change was noted at heights of 0 and 27 cm in the closed system while in the open system, due to the absorption of external water from the Mariotte bottle, the water contents are relatively higher. At a height of 51 cm, the water content declined due to the unavailability of external water in the closed system. However, in the open system, the water content of the soil in the same position firstly decreases and then rises, and finally, the evaporation tends to be stable. At the surface of the soil column, although only a small amount of water was supplied, the water content tends to stabilize after a rapid decline during evaporation rather than a further decrease in the closed system.

3.3.3. Salinity Profile. The time-history curves in Figures 18(a) and 18(b) indicate similar variations of salt content in the upper part of soil columns in closed and open systems, e.g., the domain range of 60-75 cm in height. Unlike the lower half of the contour in the closed system, two extreme values, including a maximum and a minimum, appear in the same domain in the open system. Interestingly, the position where the minimum value exists in the soil column in the open system is basically consistent with that in the closed system; however, the range influenced by the evaporation is larger and the minimum salt content appears a little earlier. The replenishment of water enhances the soil water potential gradient and dilutes the solution in soil pores, making the water easier to migrate upwards. Moreover, there is also a domain where soluble salts are accumulated near the bottom of the soil column in the open system. The higher

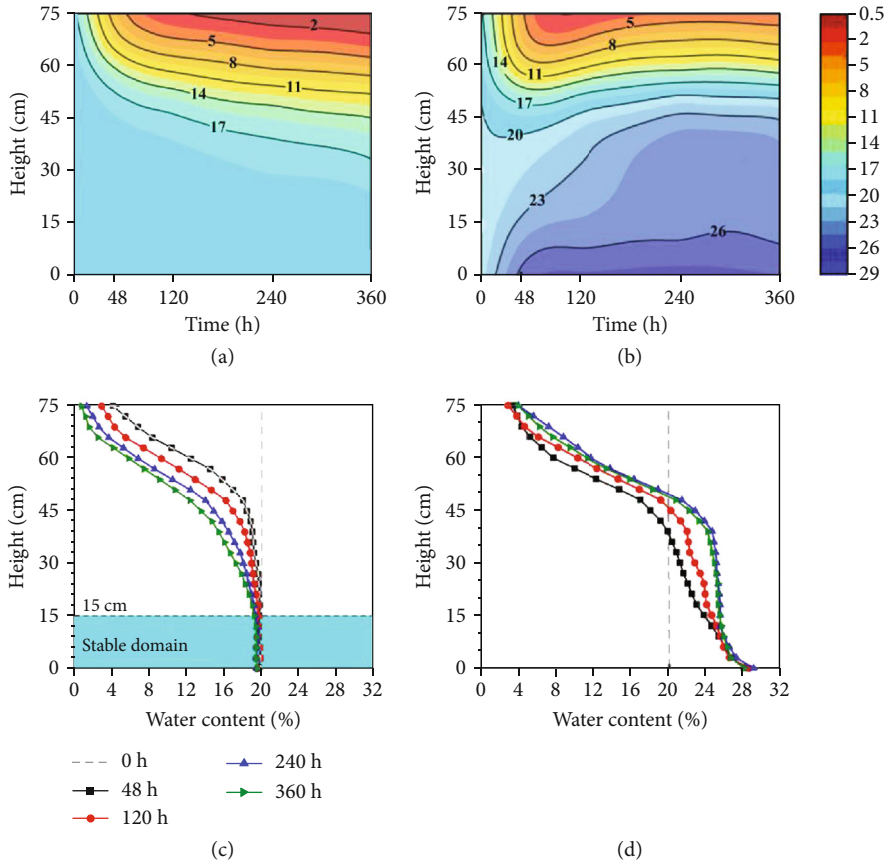

Figure 16: Water profiles during evaporation: (a) time-history curves in the closed system; (b) time-history curves in the open system; (c) profiles in the closed system; (d) profiles in the open system.

gradient between the surface of the soil column (or the phreatic water level) and the soil inside, formed in the early stage of water supply, may account for the continuous migration of solutes with water.

The profiles of salinity at five selected durations were plotted in Figures 18(c) and 18(d). Comparison of the profiles in closed and open systems show that in the early stage of evaporation, an S-shaped profile appears in the open system, which primarily originates from the precipitation of solutes in soil pores and the accumulation of migrated solutes from the soil below that were carried by capillary water. Influenced by the above two processes, two extreme values thus appear in the lower part of the soil column. The solutes in the lower part migrated further with the water as the evaporation proceeds, and the S-shaped curve tends to become smoother due to the enrichment of salts in the upper part. In the later stage, the salt accumulated at the evaporation surface further lowers the gradient of osmotic pressure, coupled with the effect of salt shell, weakening the migration of water. Thus, an abrupt transition occurs in the profile.

The variations of salt content at the selected positions of the soil column, i.e., $h = 0$, 27, 51, and 75 cm, are presented in Figure 19. At the bottom of the soil column, the water lies in a stable domain without water replenishment, and the water and salt contents are basically consistent. However, in the open system, the water that carries salt in the area is constantly moving upwards, so the curve is continuously reduced. At a height of 27 cm, the soil in the open system first undergoes the replenishment of water from the lower part due to the capillary action. Then, the evaporation process initiates in this domain, and the curve first rises and then falls, while in the closed system the salt content of the soil decreases due to the evaporation. The soil at a height of 51 cm, after evaporating for a certain period, is fully replenished by the lower water and salt, and the curve first drops and then rises. At the soil surface, the two curves change basically the same, but in the open system, the evaporation amount is larger, and correspondingly, more salts are accumulated.

3.3.4. Water Supply Intensity. Figure 20 illustrates the variation of the water supply intensity during evaporation in the open system. Three stages can be classified from the measured curve, as shown in Figure 20(a). The first is the initial water supply stage (0-78 h), characterized by a pronounced rise of capillary water, with the rate dependent on the initial water content while meteorological factors exhibit limited influence. In the soil column, a higher gradient of soil water potential is formed between the phreatic level and the soil inside, which causes a rapid rise in the capillary water content. However, this gradient declines over time with a lower intensity of water supply correspondingly. In the second stage (78-240 h), the gradient of soil water potential increases rapidly after a certain period of evaporation. Due to the

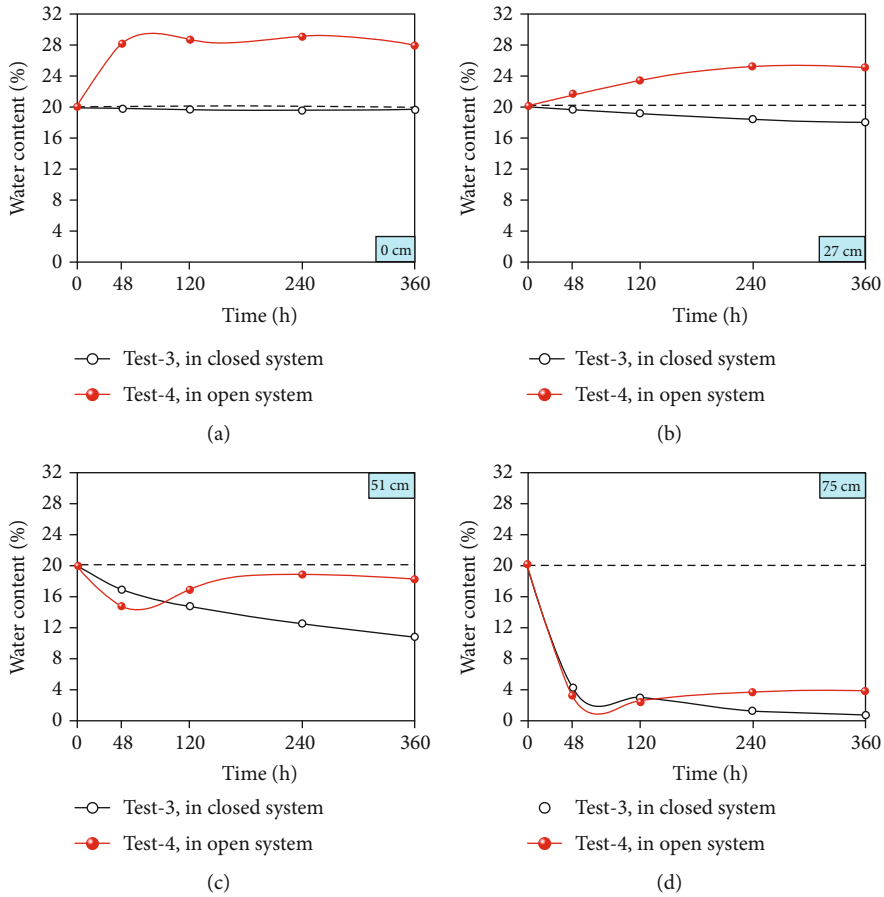

Figure 17: Variations of water content at a specific position.

hysteresis behavior of the migrated water, the delayed water supply further enhances this gradient, which leads to a rapid rise of the curve. However, as the evaporation continues, the intensity of water supply is declined. In stage III (240-360 h), the replenishment of water will continuously raise the evaporation surface, and the salt will accumulate with the water, resulting in the high salt concentration in this domain. Although the decrease in osmotic pressure leads to a higher gradient of soil water potential, the salt shell obviously reduces the water permeability. Overall, the migration of water is slowed down, resulting in a lower intensity of water supply. It should be pointed out that during the whole evaporation process the hydraulic conductivity of the soil has changed greatly. At the bottom of the soil column, due to the sufficient supply of water and the loss of salt, the soil hydraulic conductivity is very high. However, the closer to the top, the higher the salt content, resulting in a rapid decrease in the water conductivity of the soil. It is very difficult for water migration and leads to a decrease in the third stage of water supply intensity curve in Figure 20(a).

From Figure 20(b), the soil close to the heat source shows a larger variation of temperature in the three stages while little change is observed in the lower part, which mainly results from the heat capacity increase due to the absorption of external water at a lower temperature. The water and salt profiles, presented in Figures 20(c) and 20(d), show significant changes over time in the initial water supply stage. Accumulation of soluble salts, accompanied with water movement, produces a peak of the profile in the lower part of the soil column. Besides, more water is transported to the lower half of the soil column and then moves upwards and participated in the evaporation. Thus, the water content of the soil in the upper part grows insignificantly while a more pronounced change in the lower part is observed. The development of the salinity field is more complex due to the coupled transport of water and solutes. The peak salt content in the lower part of the soil column gradually disappears, and the solute continuously migrates to the upper part. A higher content of salt occurs in the upper part, which leads to the disappearance of the peak in this domain. Overall, the distribution of the entire salinity field tends to be flat. In the third stage, the evaporation tends to stabilize with a small amplitude of variation, while the soluble salt is continuously accumulated with the water to the upper part, with the salt content in the lower part decreasing. However, due to the excessive enrichment of salt at the evaporation surface, the salt shell greatly reduces the driving force of water migration, resulting in a small increase in the upper salt content.

3.4. Analysis of Coupled Transport of Heat, Water, and Solute. The heat transfer and water and salt migration in the evaporation process interact to form a complex system. In order to reveal the mechanism of this multifield coupling process, it is necessary to analyze the profiles of temperature, water,

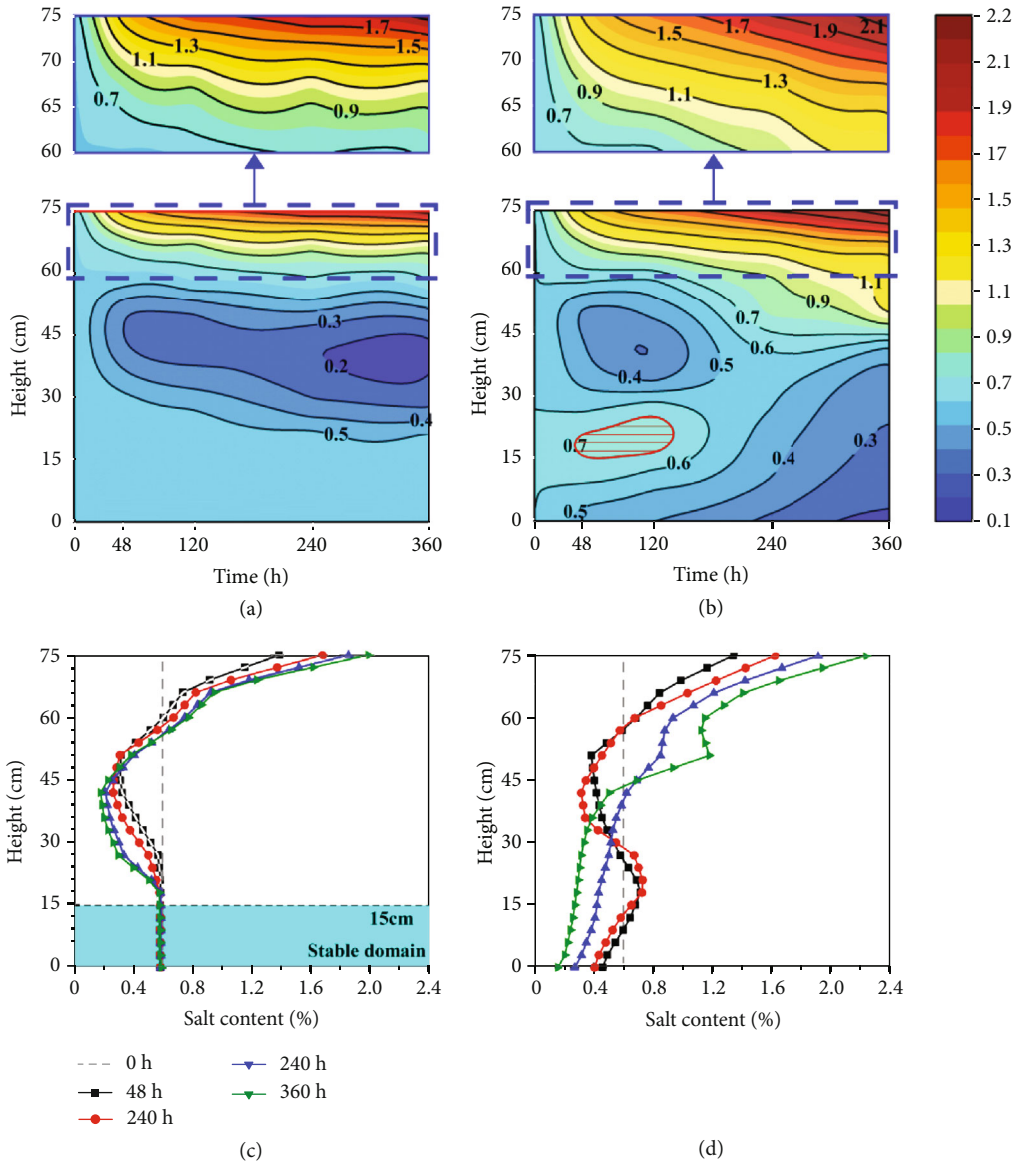

Figure 18: Salinity profiles of the soil column during evaporation: (a) time-history in the closed system; (b) time-history in the open system; (c) profile in the closed system; (d) profile in the open system.

and salt contents in the same coordinate system. Three dimensionless parameters are defined to represent the three physical fields.

$$\begin{cases} \tilde{T} = \dfrac{T}{T_0}, \\ \tilde{W} = \dfrac{W}{W_0}, \\ \tilde{\eta} = \dfrac{\eta}{\eta_0}, \end{cases} \tag{2}$$

where T is temperature (°C); T_0 is the initial temperature of the soil column (°C), taken as the mean value of the initial temperature at various test conditions, equal to 19.1°C; W is the water content (%); W_0, is the initial water content, equal to 20%; η is the salt content (%); η_0 is the initial salt content, equal to 0.6%.

Figure 21 presents the profiles of temperature, water, and salt contents after evaporation for 360 h at each test condition. In the closed system, the three profiles exhibit basically consistent changes, and clearly, both the water and salt contents vary significantly in an identical domain where a substantial change in temperature occurs. Besides, the magnitude of the extreme value and its position both decrease at higher radiation and wind speed. In the open system, due to the water supply, the water content at the bottom of the soil column increases by 50% while the salt content grows by about 3 times at the surface.

The above law reveals that temperature is an important cause of evaporation and migration of water. The migration of water will cause the salt to spread with the movement of

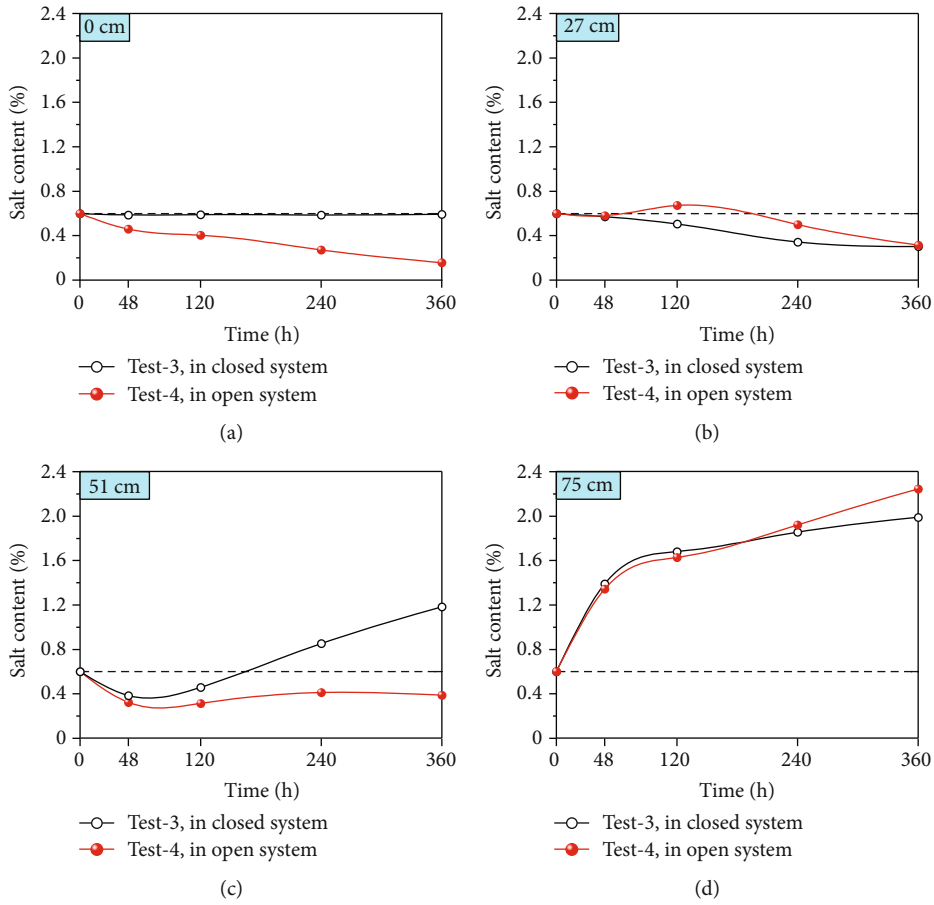

Figure 19: Variations of salt content at a specific position.

water, i.e., convection. Changes in salt migration, crystallization, and evaporation in turn affect the change in the temperature profile of the soil column. Therefore, the coupled transport of temperature, water, and salt during evaporation is a simultaneous and interactive process that occurs in soil columns.

4. Discussions

4.1. Evaporation Process of Water in Soil. Soil evaporation, in general, can be divided into three main stages [39]. Firstly, the water content of the surface soil is greater than the field capacity, and thereby, the actual evaporation is very close to the potential. Then, the actual evaporation declines approximately linearly with the decrease of soil moisture while the soil water content is less than the field capacity. Finally, the capillary path ruptures owing to the further loss of the moisture; the actual evaporation is inclined to stop. Figure 22 describes the three stages of water evaporation in the soil. In the first stage, evaporation always begins at the soil surface where the energy transferred in the form of latent heat. The main evaporation consumption in this stage is the gravity water, which is the part between the field moisture capacity and the saturation moisture capacity of the soil. When the gravity water in the surface soil has been evaporated, the moisture from the lower part will migrate upward along the capillary path to supply the evaporation on the upper part as can be noticed from Figure 22(a). If the water supply from the lower part is sufficient, the evaporation front will remain on the surface of the soil column. Otherwise, evaporation will proceed to the next stage. Due to the sufficient supply, the evaporation in this stage is mainly controlled by external factors, which is very close to the potential evaporation and has the highest intensity in the whole process.

In the second stage, the upper soil evaporates the water in the capillary path, then the evaporation front moves downward immediately. When the moisture is furthermore reduced, the capillary path to the topsoil will be broken as presented in Figure 22(b). The evaporation intensity in this stage declines approximately linearly with the decrease of soil moisture.

In the third stage, as the evaporation proceeds, the evaporation front has moved to the inside of the soil column rather than remains on the surface. When the capillary water of the topsoil is evaporated, only the bound water remains in this area. The strong bound water is tightly constrained to the soil surface and cannot move under the action of gravity and capillary. The weakly bound water is adsorbed on the outside of the strong combined water, which can move along the surface of the soil particle at an extremely low speed. As the evaporation proceeds, the weakly and the strong water are consumed, which leads to the further reduction of water content. Evaporation in the form of liquid water decreases rapidly due to multiple reasons such as the soil and the pore

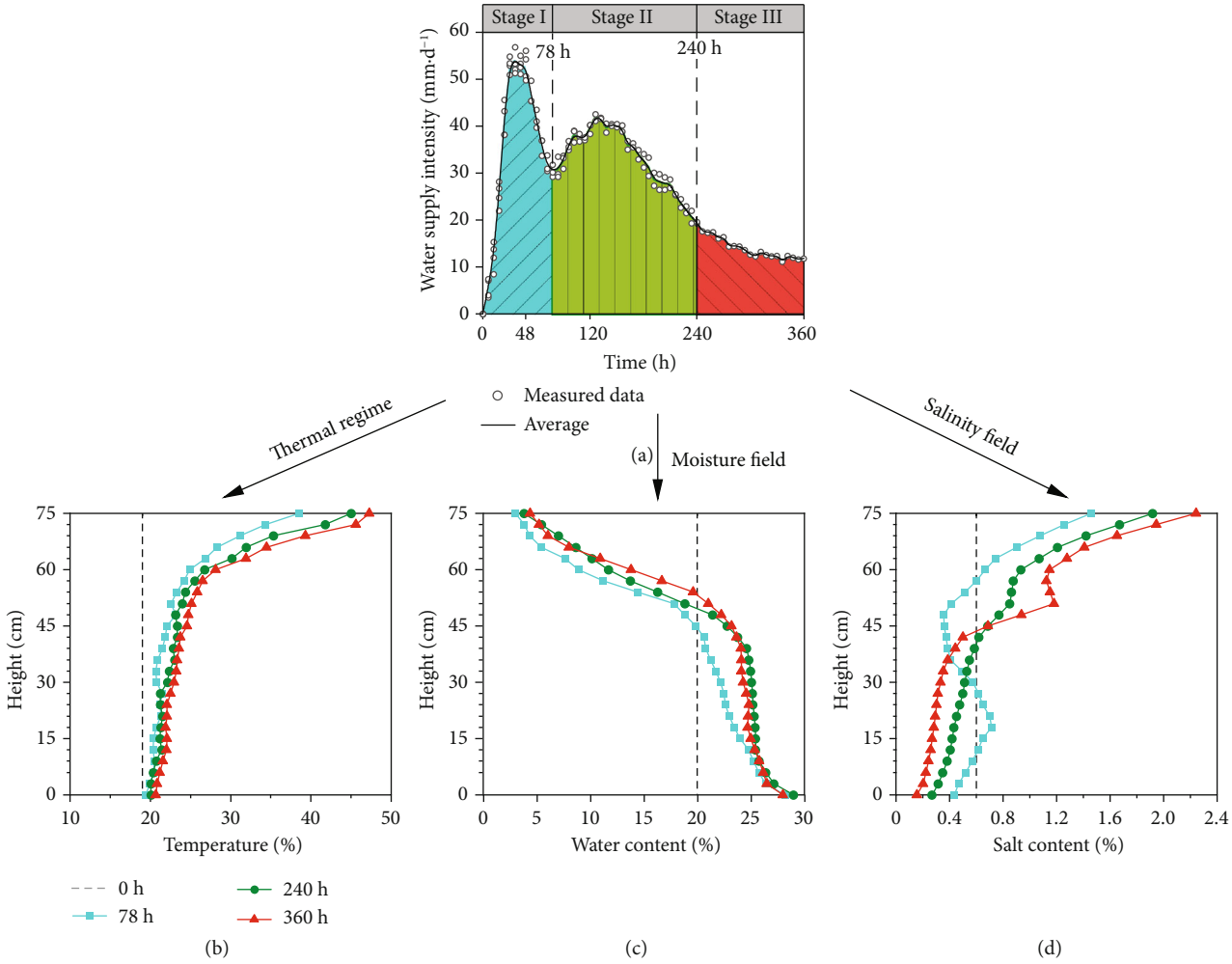

Figure 20: Variation of water supply intensity over time.

path shrink caused by the high suction, the migration driving force decreases with the reduction of suction gradient and vapor pressure gradient at the soil-air interface, and the accumulated crystal of the salt and the increase of closed bubbles lead to a large decline in permeation rate. Thus, evaporation of water in the soil column is mainly through the diffusion of vapor water in this stage. The water molecules in the form of diffusion escaping from the low part pass through the capillary fracture domain to reach the atmosphere with a quite low speed. It is worth noting that, as shown in Figure 22(c), there is still a tiny minority of strong bound water due to the strong adsorption of clay particles.

The above analysis illustrates that the soil evaporation is very closely related to the two critical water contents, which are the field moisture capacity and the capillary fracture moisture content. In addition to atmospheric evaporation capacity (such as radiation intensity, temperature, wind speed, and relative humidity), these two are the key control limits for the development of soil evaporation process, depending on the physical composition of the soil itself.

4.2. Field Moisture Capacity and Capillary Fracture Moisture Content. In order to study the effect of salinity on the two key limits, we used the Wilcox method (WM) [40] to obtain field moisture capacity under different salt content (0%, 0.6%, 1.2%, and 1.8%). With the purpose of minimizing the error, a group of parallel samples was set up and the field water holding capacity was obtained by taking the average values of the two groups of experimental results.

Figure 23 illustrates that the field moisture capacity increases almost linearly with salt content within the considered range. Previous work proves that the capillary fracture moisture content can be taken as 60% of the field moisture capacity [39] and the relationship between capillary fracture moisture and salt content can be described as

$$\theta_k = 0.6W_k = 0.318\eta + 10.872, \quad (3)$$

where θ_k (%) is the capillary fracture moisture content; W_k (%) is the field moisture capacity; η (%) is the salt content.

Equation (3) also indicates that salt has a significant effect on soil moisture capacity and determines the evaporation process, which is responsible for the large difference from the process of conventional soil. The coexistence of matric suction and osmotic suction in saline soil is an objective fact. Compared with conventional soil, the influence of osmotic

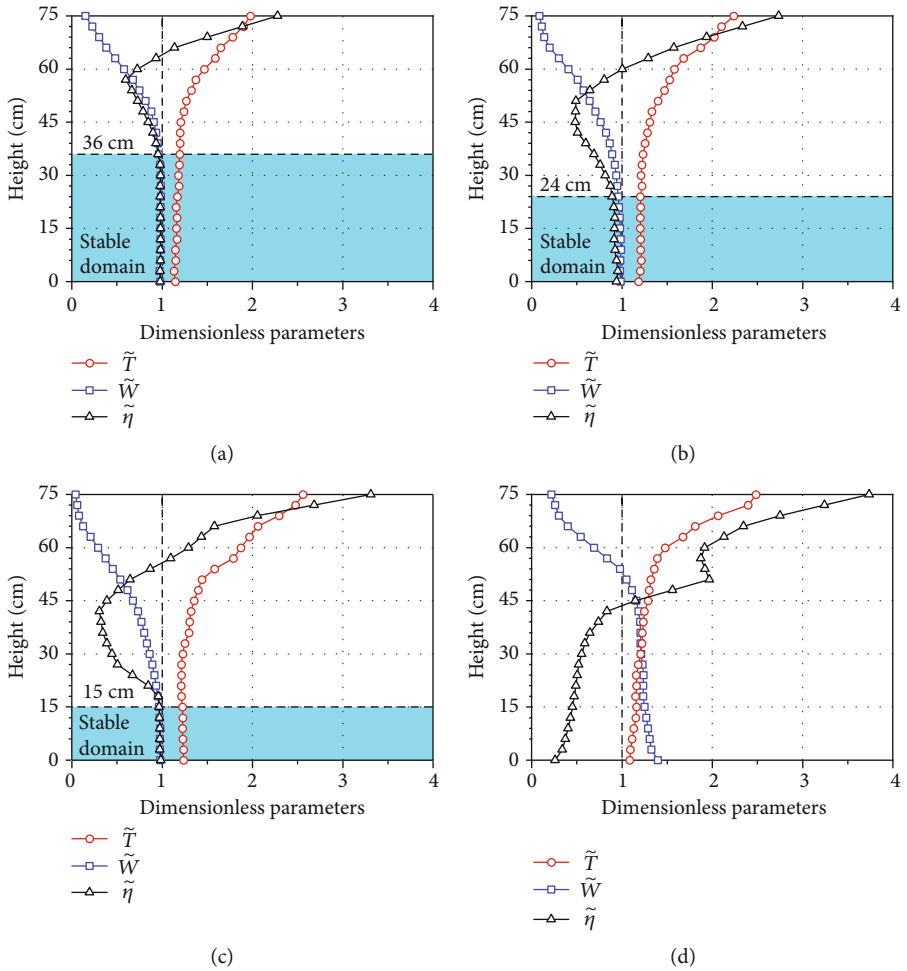

Figure 21: Temperature, water, and salt profiles after evaporation for 360 h: (a) Test 1; (b) Test 2; (c) Test 3; (d) Test 4.

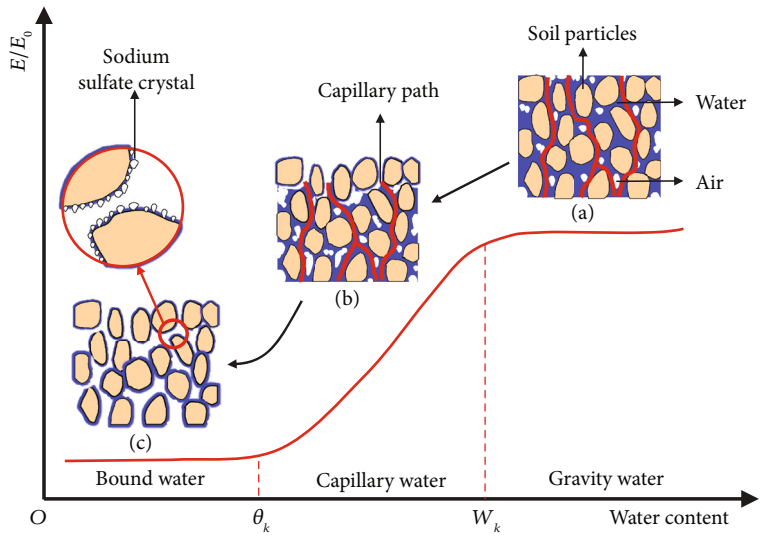

Figure 22: Evaporation process of water in soil.

components results in the increase of saline soil's moisture capacity. The higher the salt content, the greater the osmotic suction and the stronger the soil moisture capacity [41, 42]. In particular, for the large size soil column adopted in this paper, the matric and osmotic suction at each layer will affect the moisture capacity and the evaporation of the soil column along with the continuous water and salt migration, which will be discussed in detail in the next section.

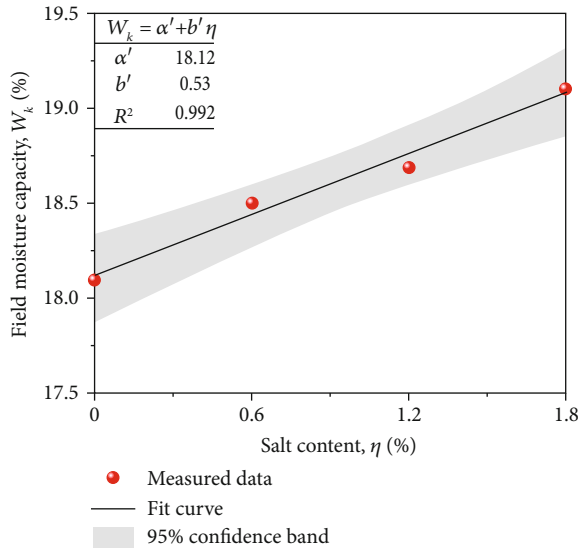

Figure 23: Field moisture capacity of loess at considered salt contents.

4.3. Discussion on the Suction Profile and Capillary Fracture Domain in Soil Columns. Total soil suction quantifies the thermodynamic potential of soil pore water relative to a reference potential of free water [43]. Neglecting temperature and gravity, the primary mechanisms that decrease the potential of soil pore water include capillary effects, short-range adsorption effects, and osmotic effects. Capillary effects are closely related to the curvature of the air-water interface and the associated negative pore water pressures in the three-phase unsaturated soil system. Short-range adsorption effects arise primarily from electrical and van der Waals force fields occurring within the vicinity of the solid-liquid interface, and the adsorbed pore water is primarily in the form of thin films coating the particle surfaces. Osmotic effects are the result of dissolved solutes in the pore water. The former mechanism is unique to unsaturated soil. The latter two may occur under either saturated or unsaturated conditions. Suction arising from the combined effects of capillarity and short-range adsorption is usually grouped under the more general term matric suction. Suction arising from the presence of dissolved solutes is referred to as osmotic suction. Total soil suction is generally considered the algebraic sum of the matric and osmotic components.

Based on the total suction test results of sodium sulfate saline loess in the same area by noncontact method [44], ignoring the interaction between matric and osmotic suction, and through multivariate fitting regression calculation, the empirical relationship among total suction, water, and salt content can be written as

$$\log S = -0.11\eta - 0.17W + 4.92, \quad (4)$$

where S (kPa) is the total suction; η (%) is the salt content; W (%) is the water content.

Figure 24(a) exhibits a good fitting effect of the equation. The measured data points lie very close to the fitted curve surface, with regression coefficients higher than 0.99 and fitting residual error between 0.794 and 1.585 kPa as plotted in Figure 24(b).

Figure 25 describes the profiles of total suction for soil columns through equation (4) under four different tests. The variations of total suction along the depth in the closed system are basically the same, at the bottom of the column, i.e., stable domain; the total suction hardly changes, while in the evaporation domain, it rises quickly with the decrease of moisture and the increase of salinity. In the open system, by contrast, the water content of the bottom soil rises rapidly by virtue of the direct effect of water supply, and thereby, the salt has been gradually displaced with the water to cause a reduction in the salt content, which results in a great decrease of the total suction in this domain. In the upper part of the soil column, the total suction rises at the beginning of evaporation and reaches its maximum after 120 h, and then, it declines quickly by cause of the gradual manifestation of the water supply.

It should be noted that in the middle and later periods of evaporation, although the total suction gradient in the upper part of the soil column is extremely high whether it is in the closed or open system, the evaporation in this domain has a tendency to stop. Consequently, the concept of the capillary fracture domain is proposed to describe the migration characteristics of soil water and salt in this domain. By combining equation (3) and equation (4), the relationship between the critical value of total suction and salt content can be deduced as

$$\log S_k = -0.11\eta^2 + 0.36\eta + 3.07, \quad (5)$$

where S_k (kPa) is the total suction corresponding to the capillary fracture moisture content; η (%) is the salt content. If $\log S \geq \log S_k$, it indicates that the area is located in the capillary fracture domain.

Figure 26 presents the time-history curves for total suction under four different tests, which depend on the results of water and salt transfer in the soil column. In the capillary fracture domain, although the total suction is very high, the capillary water has been evaporated, and the bound water adsorbed tightly on the surface of the soil particles is difficult to move. In addition, the fracture of the capillary pathway makes it tough for the water from the lower part to move upward. For many reasons, the evaporation in the form of vapor water diffusion dominates, but its diffusion rate is much lower than the previous capillary water migration. However, as a result of the sufficient water supply in the open system, a continuous capillary path can be formed by repairing the capillary fracture domain due to the insufficient water supply at the beginning of evaporation in a certain way, which leads to the upward movement of the evaporation front, i.e., the depth of the fracture domain shown in Figure 26(d) rises first and then decreases.

The above law reveals that the core area of evaporation lies in the capillary fracture domain. In spite of the high suction and suction gradients, there is no continuous capillary path, which has little effect on the water and salt migration in the soil column. Moreover, it should be pointed out that

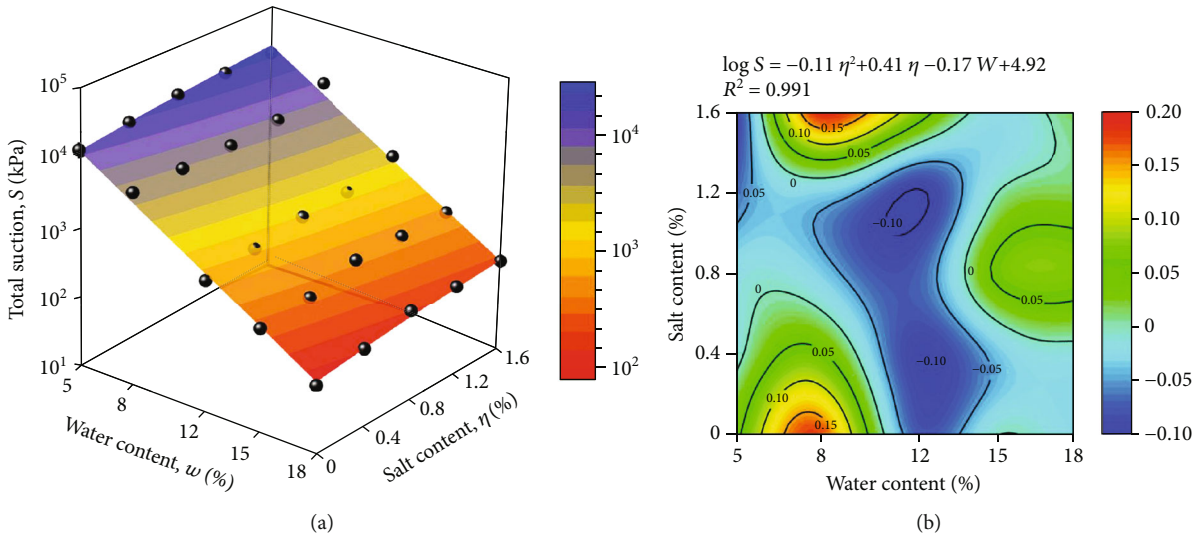

Figure 24: Total suction and fitting residual error.

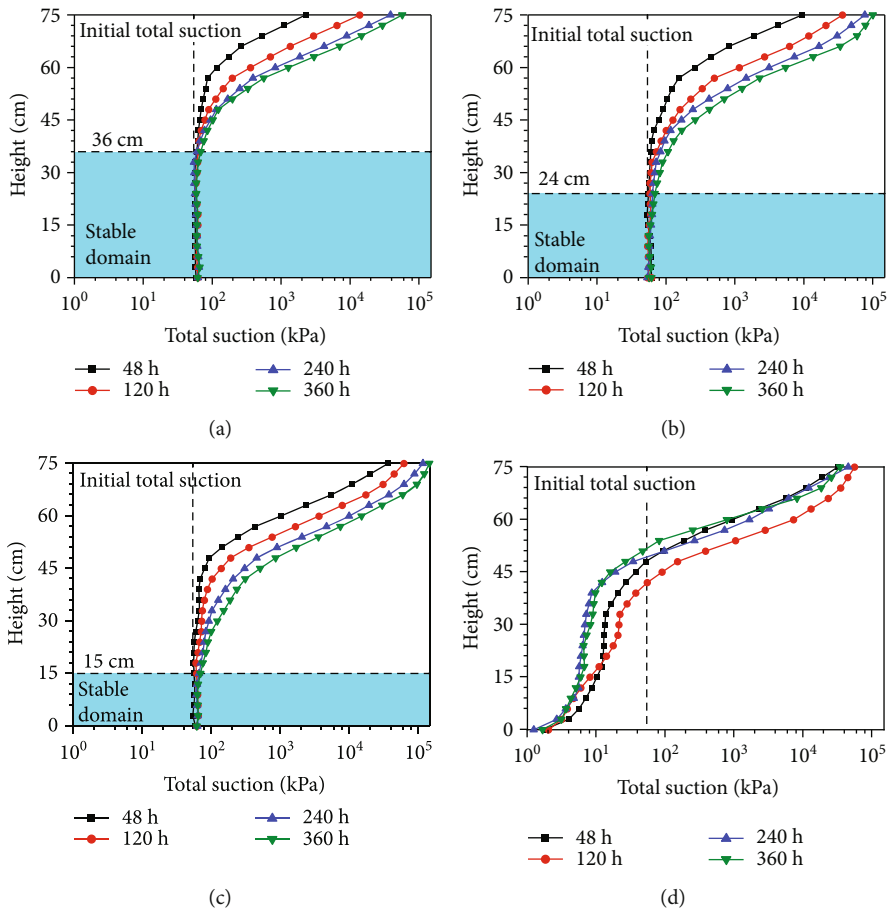

Figure 25: Total suction profile: (a) Test 1; (b) Test 2; (c) Test 3; (d) Test 4.

in this domain, the salinity is highly enriched, the moisture is much lower than the effective water absorbed by the plant, and the soil structure is very loose. The influence of the capillary fracture domain should be taken into consideration in practical industrial- and agricultural-related issues.

5. Conclusions

This paper carried out laboratory experiments on the evaporation characteristics of loess columns and water-solute coupled transport induced by evaporation. Three test conditions in the

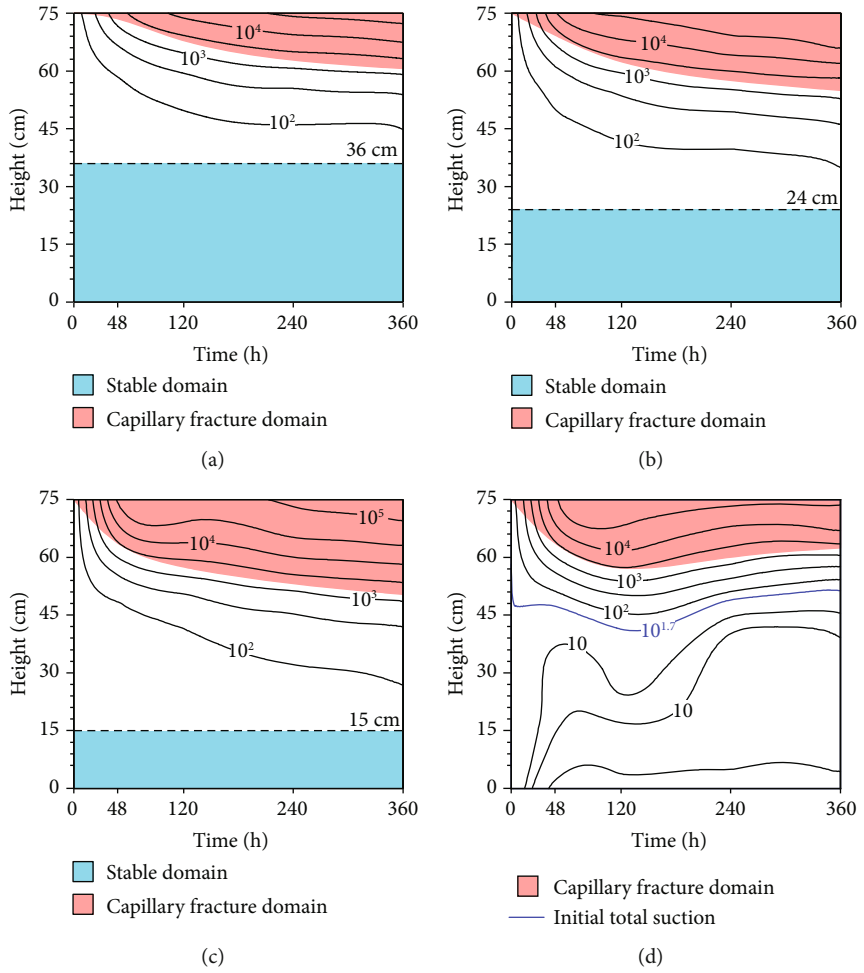

Figure 26: Time-history of total suction: (a) Test 1; (b) Test 2; (c) Test 3; (d) Test 4.

closed system and one group in the open system as a comparison were considered. Based on the variation of total suction and moisture content at capillary rupture, a criterion judging the capillary fracture area was proposed and the development of the three physical fields was further discussed. The main conclusions are as follows.

(1) Meteorological factors exhibit significant effects on the evaporation of soil columns. The evaporation-affected domain increases at higher radiation intensity and wind speed. The evaporation coefficient can well characterize the evaporation capacity of the soil. In the closed system, the evaporation coefficient varies insignificantly while in the open system it first decreases and then grows

(2) There is an evaporation stable domain in the soil column in the closed system, where the temperature, water, and salt profiles show little change. At higher radiation intensity and wind speed, a larger amount of evaporation occurs with a lower water content at the surface but a higher salt content. In the open system, three stages were noted from the process of water supply. The water supply intensity tends to stabilize even when some abrupt changes were found from the measured curves

(3) The capillary fracture area in soil columns is the core area for soil evaporation and lies at a higher position after a longer duration or at a higher intensity of evaporation. In the open system, due to the sufficient supply of external water, the capillary fracture area can be fixed, so that the height of this area first increases and then decreases

(4) The variation of temperature gradient results in a higher gradient of matric potential at soil surface, which further leads to the migration of water. This will in turn cause the salt to migrate with the water, i.e., the convective diffusion. The migration and later crystallization of salt will lead to the changes in temperature profile during evaporation. Therefore, the coupled transport of heat, water, and salt during evaporation is an interactive and complex process

Data Availability

The data used to support the findings of this study are available from the corresponding author upon request.

Conflicts of Interest

The authors declare that there is no conflict of interest regarding the publication of this paper.

Acknowledgments

The research described in this paper was financially supported by the National Natural Science Foundation of China (Nos. 51878551 and 51478385). These supports are greatly appreciated.

References

[1] C. L. Zhao, M. A. Shao, X. X. Jia, C. C. Zhang, X. X. Jia, and C. C. Zhang, "Particle size distribution of soils (0–500 cm) in the Loess plateau, China," *Geoderma Regional*, vol. 7, no. 3, pp. 251–258, 2016.

[2] H. Shi and M. Shao, "Soil and water loss from the Loess Plateau in China," *Journal of Arid Environments*, vol. 45, no. 1, pp. 9–20, 2000.

[3] Z. Jin, L. Guo, Y. Wang et al., "Valley reshaping and damming induce water table rise and soil salinization on the Chinese Loess Plateau," *Geoderma*, vol. 339, no. 1, pp. 115–125, 2019.

[4] X. T. Xu, Y. B. Wang, R. Q. Bai, H. W. Zhang, and K. Hu, "Effects of sodium sulfate content on mechanical behavior of frozen silty sand considering concentration of saline solution," *Results in Physics*, vol. 6, pp. 1000–1007, 2016.

[5] X. T. Xu, Y. B. Wang, Z. H. Yin, and H. W. Zhang, "Effect of temperature and strain rate on mechanical characteristics and constitutive model of frozen Helin loess," *Cold Regions Science and Technology*, vol. 136, pp. 44–51, 2017.

[6] J. Xu, X. Zheng, and Z. Q. Wang, "Investigation for water and salt migrations on spalling disease of loess slope caused by salificatifon erosion," *Journal of Engineering Geology*, vol. 26, no. 3, pp. 741–748, 2018.

[7] S. H. Wang, Q. Z. Wang, J. L. Qi, and F. Y. Liu, "Experimental study on freezing point of saline soft clay after freeze-thaw cycling," *Geomechanics and Engineering*, vol. 15, no. 4, pp. 997–1004, 2018.

[8] J. B. Han, J. Lin, and Y. F. Dai, "Numerical modeling of soil evaporation process and its stages dividing during a drying cycle," *Geofluids*, vol. 2017, Article ID 5892867, 11 pages, 2017.

[9] J. Fan, W. Yue, L. Wu et al., "Evaluation of SVM, ELM and four tree-based ensemble models for predicting daily reference evapotranspiration using limited meteorological data in different climates of China," *Agricultural and Forest Meteorology*, vol. 263, pp. 225–241, 2018.

[10] D. A. Rose, F. Konukcu, and J. W. Gowing, "Effect of watertable depth on evaporation and salt accumulation from saline groundwater," *Australian Journal of Soil Research*, vol. 43, no. 5, pp. 565–573, 2005.

[11] D. W. Huang, J. S. Chen, L. C. Zhan, T. Wang, and Z. G. Su, "Evaporation from sand and loess soils: an experimental approach," *Transport in Porous Media*, vol. 113, no. 3, pp. 639–651, 2016.

[12] X. Lu, Y. Ju, L. Wu, J. Fan, F. Zhang, and Z. Li, "Daily pan evaporation modeling from local and cross-station data using three tree-based machine learning models," *Journal of Hydrology*, vol. 566, pp. 668–684, 2018.

[13] J. L. Fan, K. T. Oestergaard, A. Guyot, and D. A. Lockington, "Estimating groundwater recharge and evapotranspiration from water table fluctuations under three vegetation covers in a coastal sandy aquifer of subtropical Australia," *Journal of Hydrology*, vol. 519, pp. 1120–1129, 2014.

[14] P. J. M. Cooper, J. D. H. Keatinge, and G. Hughes, "Evapotranspiration-technique for calculation of its components by field measurements," *Field Crops Research*, vol. 7, pp. 229–312, 1983.

[15] Z. Y. Wang and J. F. Chen, "Discussion on calculating soil water balance elements by zero flux surface method," *Underground Water*, vol. 24, pp. 141-142, 2002.

[16] G. Y. Qiu, T. Yano, and K. Momii, "An improved methodology to measure evaporation from bare soil based on comparison of surface temperature with a dry soil surface," *Journal of Hydrology*, vol. 210, no. 1-4, pp. 93–105, 1998.

[17] A. J. Mutziger, C. M. Burt, D. J. Howes, and R. G. Allen, "Comparison of measured and FAO-56 modeled evaporation from bare soil," *Journal of Irrigation and Drainage Engineering*, vol. 131, no. 1, pp. 59–72, 2005.

[18] F. Ventura, R. L. Snyder, and K. M. Bali, "Estimating evaporation from bare soil using soil moisture data," *Journal of Irrigation and Drainage Engineering*, vol. 132, no. 2, pp. 153–158, 2006.

[19] M. Aydin, S. L. Yang, N. Kurt, and T. Yano, "Test of a simple model for estimating evaporation from bare soils in different environments," *Ecological Modelling*, vol. 182, no. 1, pp. 91–105, 2005.

[20] J. Z. Zhou, C. F. Wei, D. Q. Li, and H. Z. Wei, "A moving-pump model for water migration in unsaturated freezing soil," *Cold Regions Science and Technology*, vol. 104, pp. 14–22, 2014.

[21] F. Ming and D. Q. Li, "A model of migration potential for moisture migration during soil freezing," *Cold Regions Science and Technology*, vol. 124, pp. 87–94, 2016.

[22] I. Braud, A. C. Dantas-Antononi, M. Vauclin, J. L. Thony, and P. Ruelle, "A simpler soil-plant-atmosphere transfer model development and field verification," *Journal of Hydrology*, vol. 166, no. 3-4, pp. 213–250, 1995.

[23] M. G. Shao, R. Horton, and D. B. Jaynes, "Analytical solution for one-dimensional heat conduction-convection equation," *Soil Science Society of America Journal*, vol. 62, no. 1, pp. 123–128, 1998.

[24] S. H. Wang, J. L. Qi, F. Yu, and X. L. Yao, "A novel method for estimating settlement of embankments in cold regions," *Cold Regions Science and Technology*, vol. 88, pp. 50–58, 2013.

[25] S. H. Wang, J. L. Qi, F. Yu, and F. Y. Liu, "A novel modeling of settlement of foundations in permafrost regions," *Geomechanics and Engineering*, vol. 10, no. 2, pp. 225–245, 2016.

[26] Y. A. Pachepsky, J. W. Craeford, and W. J. Rawls, *Fractal in Soil Science, vol. 27*, Elsevier, 2000.

[27] J. I. Freijer, T. M. Post, B. A. Ploeger, J. DeJongh, and M. Danhof, "Application of the convection–dispersion equation to modelling oral drug absorption," *Bulletin of Mathematical Biology*, vol. 69, no. 1, pp. 181–195, 2007.

[28] J. Simunek, H. Saito, M. Sakai, and M. T. G. Van, *The Hydrus-1D Software Package for Simulating the One-Dimensional Movement of Water, Heat, and Multiple Solutes in Variably-Saturated Media, Version 4.0*, US Salinity Laboratory, California, 2008.

[29] M. B. Huang and J. Gallichand, "Use of the SHAW model to assess soil water recovery after apple trees in the gully region of the Loess Plateau, China," *Agricultural Water Management*, vol. 85, no. 1-2, pp. 67–76, 2006.

[30] I. N. Nassar and R. Horton, "Water transport in unsaturated nonisothermal salty soil: I. Experimental results," *Soil Science Society of America Journal*, vol. 53, pp. 1323–1329, 1989.

[31] I. N. Nassar and R. Horton, "Water transport in unsaturated nonisothermal salty soil: II. Theoretical development," *Soil Science Society of America Journal*, vol. 53, no. 5, pp. 1330–1337, 1989.

[32] J. Bear and A. Gilman, "Migration of salts in the unsaturated zone caused by heating," *Transport in Porous Media*, vol. 19, pp. 139–156, 1995.

[33] X. Z. Xu, J. C. Wang, and L. X. Zhang, *Frozen Soil Physics*, Science Press, Beijing, China, 2001.

[34] D. Y. Wu, X. Y. Zhou, and X. Y. Jiang, "Water and salt migration with phase change in saline soil during freezing and thawing processes," *Ground Water*, vol. 56, pp. 742–752, 2018.

[35] X. S. Wan, F. M. Gong, M. F. Qu, E. X. Qiu, and C. M. Zhong, "Experimental study of the salt transfer in a cold sodium sulfate soil," *KSCE Journal of Civil Engineering*, vol. 23, no. 4, pp. 1573–1585, 2019.

[36] W.-C. Cheng, W. Lin, Z.-F. Xue, J. C. Ni, M. Rahman, and A. Arulrajah, "Lubrication performance of pipejacking in soft alluvial deposits," *Tunnelling and Underground Space Technology*, vol. 91, article 102991, 2019.

[37] W.-C. Cheng, J. C. Ni, A. Arulrajah, and H.-W. Huang, "A simple approach for characterising tunnel bore conditions based upon pipe-jacking data," *Tunnelling and Underground Space Technology*, vol. 71, pp. 494–504, 2018.

[38] J. J. Chen, *The Research on the Land Surface Evapotranspiration of Loess and the Laws of Soil Water Movement in Arid Environment, [M.S. Thesis]*, Xi'an University of Architecture and Technology, China, 2014.

[39] X. F. Rui, *Principles of Hydrology*, China Water & Power Press, Beijing, China, 2004.

[40] X. Duan, Y. Xie, G. Liu, X. Gao, and H. Lu, "Field capacity in black soil region, Northeast China," *Chinese Geographical Science*, vol. 20, no. 5, pp. 406–413, 2010.

[41] M. Mizoguchi, "A deviation of matric potential in frozen soil," *Bulletin of the Faculty of Bioresources Mie University*, vol. 10, pp. 175–182, 1993.

[42] D. Sun, J. Zhang, and G. Song, "Experimental study of soil-water characteristic curve of chlorine saline soil," *Rock and Soil Mechanics*, vol. 34, no. 4, pp. 955–960, 2013.

[43] N. Lu and W. J. Likos, *Unsaturated Soil Mechanics*, John Wiley & Sons, Inc, Hoboken, NJ, USA, 2000.

[44] X. S. Mao, T. D. Zhang, F. F. Liu, and Y. Y. Li, "Experimental study of osmotic suction of sulphate saline soil based on soil-water characteristic curve," *Journal of Xi'an University of Architecture and Technology (Natural Science Edition)*, vol. 51, no. 1, pp. 27–41, 2019.